LAMK Lahden ammattikorkeakoulu
Lahti University of Applied Sciences

MEASURING FLOW RATE OF MIXTURE GASES

Developing a digital gas flow meter for industrial welding solutions

LAHTI UNIVERSITY OF APPLIED SCIENCES
Degree Programme in Digital Technologies
Master's Thesis
Spring 2017
Tuomas Terho

Lahti University of Applied Sciences
Degree Programme in Digital Technologies

TERHO, TUOMAS:

Measuring flow rate of mixture gases:
Developing a digital gas flow meter for industrial welding solutions

Master's Thesis

83 pages

Spring 2017

ABSTRACT

Shielding gases that are used in fusion welding are typically mixtures of up to three of the following six industrial pure gases: argon, helium, carbon dioxide, hydrogen, nitrogen and oxygen. There are tens of different mixtures on the market and the amount is continuously developing along with welding processes and materials. Currently a gas flow meter that would adapt with any mixture and that would be designed to meet welding requirements does not exist. The objective of this study is to develop a new gas flow meter device that would measure gas flow rate for any percentage-level mixture of the pure gases used in welding.

This study utilized the methods of applied science. Gas flow physics were researched on kinematics and thermodynamics fields: kinematics to construct a suitable mechanical flow system for mixture gases, and thermodynamics to discover a method to measure the flow rate of mixture gases. The research phase contained both theoretical and experimental studies. The development phase contained design and implementation of mechanics, electronics and software. In the electrical circuit a thermal mass flow sensor was connected to a microcontroller unit as a constant temperature anemometer. Mass flow characteristic curves for the pure welding gases were measured and were pre-programmed into microcontroller's software. In the software a programmatic algorithm was developed to apply the thermodynamics theory to the measured mass flow values for the volumetric flow rate calculation.

This research disclosed a new simple method to combine the physical properties of pure gases, yielding corresponding properties for mixtures. The method took advantage of the thermal mass flow sensor and the constant temperature anemometer circuitry. However, the research revealed that the constant temperature anemometer is significantly sensitive to the variation in the gas temperature and in the temperature of the sensor housing. Although the new method was found accurate in stable temperature conditions, compensation of the temperature variation requires further investigation for the final product. That investigation is not included in this study.

Key words: arc welding, gas flow meter, laminar flow, mass flow, mixture gas, shielding gas, thermal mass flow sensor, thermodynamics, volumetric flow

Lahden ammattikorkeakoulu
Digitaaliset teknologiat

TERHO, TUOMAS:

Seoskaasujen virtauksen mittaaminen:
Digitaalisen kaasunvirtausmittarin kehittäminen teollisiin hitsausratkaisuihin

Opinnäytetyö, YAMK

83 sivua

Kevät 2017

TIIVISTELMÄ

Sulahitsauksessa käytetään suojakaasuja, jotka ovat tyypillisesti seuraavien kuuden teollisuudessa käytetyn puhtaan kaasun seoksia: argon, helium, hiilidioksidi, vety, typpi ja happi. Markkinoilla on kymmeniä seoskaasuja, ja määrä lisääntyy koko ajan hitsausprosessien ja hitsattavien materiaalien kehityksen myötä. Tällä hetkellä ei ole olemassa kaasunvirtausmittaria, joka pystyisi mittaamaan mitä tahansa seoskaasua ja joka täyttäisi hitsauksen asettamat vaatimukset. Tämän työn tavoitteena on kehittää uusi kaasunvirtausmittari, joka mittaa kaasun virtausmäärän mille tahansa prosenttitason hitsauskaasuseokselle.

Tässä työssä käytettiin sovelletun tutkimuksen menetelmiä. Kaasunvirtausfysiikkaa tutkittiin kinematiikan ja termodynamiikan osa-alueilla: kinematiikkaa mekaanisen virtausjärjestelmän rakentamiseksi seoskaasuille, ja termodynamiikkaa seoskaasujen virtausmittausmenetelmän löytämiseksi. Tutkimusvaihe sisälsi sekä teoreettista että kokeellista tutkimusta. Kehitysvaihe sisälsi mekaniikan, elektroniikan ja ohjelmiston suunnittelua ja kehittämistä. Elektronisessa kytkennässä lämpömassavirta-anturi kytkettiin mikro-ohjaimeen vakiolämpöanemometriksi. Puhtaiden kaasujen massavirtauksen ominaiskäyrät mitattiin ja esiohjelmoitiin mikro-ohjaimen ohjelmistoon. Ohjelmistoon kehitettiin algoritmi, joka hyödynsi termodynamiikan teoriaa tilavuusvirtausnopeuden laskemiseksi mitatuista massavirtausarvoista.

Tämä tutkimus toi esille uuden menetelmän, jolla voidaan laskea puhtaiden kaasujen fyysisistä ominaisuuksista vastaavat ominaisuudet kaasuseoksille. Menetelmässä käytettiin hyväksi lämpömassavirta-anturia ja vakiolämpöanemometria. Tutkimus paljasti kuitenkin, että vakiolämpöanemometri on merkittävän herkkä kaasun lämpötilan ja anturin koteloinnin lämpötilan vaihteluille. Vaikka uusi menetelmä osoittautui tarkaksi stabiileissa lämpötilaolosuhteissa, lämpötilan muutosten kompensointi vaatii lisätutkimuksia lopputuotetta varten. Lisätutkimukset eivät sisälly tähän työhön.

Avainsanat: kaarihitsaus, kaasunvirtausmittari, laminaarinen virtaus, massavirta, seoskaasu, suojakaasu, lämpömassavirta-anturi, termodynamiikka, tilavuusvirta

CONTENTS

TERMS AND ABBREVIATIONS

A/D	Analog-to-digital
ADC	Analog-to-digital converter
Ar	Argon
ARM®	Advanced RISC (reduced instruction set computing) machines
ATM	Atmosphere (pressure, 101.3 kPa)
BGA	Ball-grid array
CAN	Computer-area network
CNC	Computerized numerical control
CO_2	Carbon dioxide
CTA	Constant temperature anemometer
FET	Field-effect transistor
GMAW	Gas metal arc welding
GND	Ground (an electrical potential)
H, H_2	Hydrogen, 2-atomic hydrogen molecule
He	Helium
IoT	Internet-of-Things
IST	Innovative Sensor Technology IST AG (a Swiss company)
M2M	Machine-to-machine
MAG	Metal active-gas welding
MCU	Micro-controller unit

MIG	Metal inert-gas welding
N, N_2	Nitrogen, 2-atomic nitrogen molecule
NO	Nitric oxide (nitrogen monoxide)
NTC	Negative temperature coefficient
NTP	IUPAC normal temperature and pressure (0°C and 100 kPa)
O, O_2	Oxygen, 2-atomic oxygen molecule
PCB	Printed circuit board
POM	Polyoxymethylene (acetal, polyacetal, polyformaldehyde)
PTC	Positive temperature coefficient
PWM	Pulse width modulation
RAM	Random access memory
RTOS	Real-time operating system
RTXC	A Quadros real-time operating system
STP	Standard temperature and pressure (typically 0°C and 101.3 kPa)
TAG	Tungsten active-gas welding
TIG	Tungsten Inert-Gas welding
VCC	Power supply voltage
WPS	Welding procedure specification

1 INTRODUCTION

Industrial gas metal arc welding (GMAW) started to develop in 1920s (Becken 1969, Preface) and it is widely used in industry nowadays. Arc welding is the most used and the most important group of welding processes in mechanical engineering. GMAW processes, such as MIG/MAG and TIG, belong to that group. (Lukkari 1997, 5.)

This study was made for Kemppi Oy, the Finnish welding equipment manufacturer and solution provider. The company is introducing a whole-new concept for welding quality management. The quality management toolbox includes equipment with IoT (internet of things) and M2M (machine-to-machine) connectivity, cloud services like data collection, real-time quality exception alert system, digital WPS (welding procedure specification), and much more (WeldEye 2016).

The quality management toolbox requires more real-time data from the welding system than never before. Kemppi's welding equipment provide a rich set of electrical properties from the welding process, which they use also by themselves for process control. However, some information like temperature and gas flow rate are not originally available in the system. To support those there has to be dedicated sensors, communicating with the Kemppi welding system. From the sensors, this requires specific capability to communication.

1.1 Requirement for a specific mixture gas flow meter

In GMAW processes weld quality is relative to a correct shielding gas flow rate and a gas type. The gas flow rate is adjusted manually by a regulator. Gas flow is typically monitored by a rotameter, the mechanical gravity-based instrument. (Phillips 1958; Lukkari 1999.)

Modern welding systems have display units or even web pages monitoring welding events and status, and collecting data. This requires digitalized information from monitored subjects. To monitor the gas flow rate, the system needs a digital gas flow meter connected directly to a data bus.

The gas flow meter should meet the following requirements to be suitable for Kemppi welding applications:

1. Measurement range, based on common knowledge in automated welding, is from 0 to 25 liters per minute in NTP (normal temperature and pressure) conditions.
2. All (or at least the most) common industrial pure gases and their mixtures used in welding are supported. The list of the pure gases is investigated in this study.
3. All information provided by the gas flow meter are digital. This means that the currently used pure gas or mixture is configured to the gas flow meter digitally, and the gas flow meter produces volumetric flow rate information digitally.
4. The mechanical size of the device is small enough to be mounted inside welding wire feeders manufactured by Kemppi.
5. The cost of the gas flow meter is on acceptable level.

The detailed examination of commercial solutions is beyond the scope of this study. In conclusion, a commercial solution which would meet all the requirements of the above list does not exist. This is origin for the requirement for a new specific mixture gas flow meter.

1.2 Research questions, objectives and scope

The objective of this study is to research and develop a gas flow meter that fulfils the requirements discussed in the previous topic. This study answers to three research questions. The first and the most important research question in this study is the following hypothetical issue:

> *How the physical properties of pure gases can be combined mathematically so that they produce corresponding physical properties for any mixture of those gases?*

To answer this question, the set of pure gases must be identified, their physical properties must be investigated, and a reciprocal physical connection between pure gases has to be examined. The second research question is:

> *How to measure gas flow such a way that the physico-mathematical connection between the pure gases can be used to solve the flow rate of a mixture gas algorithmically?*

To answer this question, different gas flow measurement methods have to be analyzed and a suitable method has to be selected. This phase includes also analysis of the electrical solution for the measurement device.

The third research question and a basis for the development phase is:

> *How to engineer a device that fulfils mechanically, electronically and programmatically the requirements listed on page 2?*

To answer this question, the gas flow meter device has to be developed based on the results of the two preceding research questions. The development phase includes mechanical design and construction, electronic component selections, electrical schematic and PCB (printed circuit board) layout design, prototyping and testing.

1.3 Theoretical frame

The theoretical frame of this study consists of gas flow physics on both thermodynamics and kinematics fields from the measurement point of view. The physics affects to the mechanical construction, to the measurement principle selection, to the electronics, and to the programmatic algorithm that calculates the gas flow rate. The study is constrained to the gases used in welding under environmental conditions that are typical for welding. A flow tube discussed in this study is assumed to be a straight, constant diameter circular pipe.

For the algorithm the following principles of the thermodynamics gas theory have to be understood:

- heat transfer by convection,
- heat conductivity of gases,
- specific heat capacity and degrees of freedom,
- gas mixing rules for real gases, and
- temperature effect to overall physical properties of gases.

To find out a suitable mechanical construction the following basic principles of the kinematic gas theory have to be understood:

- relationship between gas volume and mass,
- volumetric flow rate and velocity in a tube,
- turbulent and laminar flow and their effects in a tube, and
- flow development in a tube and its effect to entry length.

1.4 Research methods

This study is an applied research including a research phase (pilot studies) and a development phase (the main study). The pilot studies include the following tasks:

- investigation on shielding gases and flow rate requirements,
- investigation on gas flow metering methods and tools,
- selection of measurement method and components, and
- theoretical research on gas kinematics and thermodynamics.

The main study includes the following tasks:

- experimental research of the flow tube suitable for measurement,
- experimental research of the measurement electronics, and
- theoretical research and programmatic implementation of the physico-mathematical algorithm.

2 SHIELDING GASES IN GMAW WELDING

GMAW (gas metal arc welding) is a welding method where an electric arc burns between an electrode and a work piece. The arc is shielded by gas flowing out from a gas nozzle that covers the electrode (figure 1). The GMAW processes can be divided into two categories by the electrode: MIG/MAG and TIG. In the TIG (Tungsten inert gas) process the electrode is a non-consumable wolfram rod. In the MIG (metal inert gas) and MAG (metal active gas) the electrode is a consumable filler wire. (Lukkari 1997, 158.)

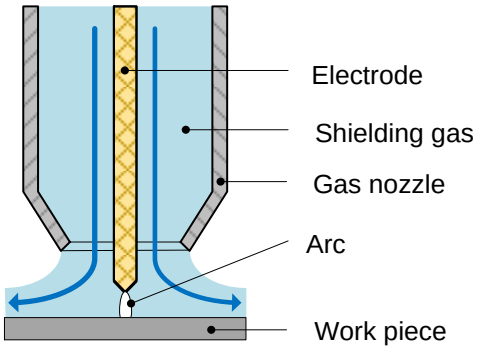

FIGURE 1. GMAW principle

According to Welding Handbook, atomic-hydrogen was the first shielding gas used in metal arc welding, and it was the best gas for metals other than low-carbon steel. Since then, shielding gases have developed and the atomic-hydrogen has been replaced by low-cost inert gases. (Phillips 1958, 26.4.)

GMAW processes require many different shielding gases that have multiple roles in the process. Basically the gases are divided into two categories, *inert* (non-reactive) and *active* (reactive). In inert mixture all components are inert, when in active mixture at least one component is active. (Lukkari 1997, 158.)

Shielding gases control heat input to the weld, reduce or increase oxidation, stabilize the arc, have cleaning action on the base material, and affect the quality of the weld. They are selected by a base material (bare metal or an alloy), by thickness of the base material, and by the desired effect. (Lukkari 1997, 196-198; Phillips 1958, 27.29-27.31.)

2.1 Pure gases and mixtures

As listed in the standard SFS-EN ISO 14175:2008 (Welding consumables: Gases and gas mixtures for fusion welding and allied processes), shielding gases are based on six industrial pure gases: argon, helium, carbon dioxide, oxygen, hydrogen and nitrogen. Argon and helium are inert gases, carbon dioxide and oxygen are oxidizing, nitrogen is low-reactive and hydrogen is reducing (table 1).

TABLE 1. Pure welding gases (SFS-EN ISO 14175:2008)

Type of gas	Chemical symbol	Density[a] (air = 1,293) kg/m^3	Relative density[a] to air	Boiling point at 0,101 MPa °C	Reactivity during welding
Argon	Ar	1,784	1,380	-185,9	Inert
Helium	He	0,178	0,138	-268,9	Inert
Carbon dioxide	CO_2	1,977	1,529	-78,5[b]	Oxidizing
Oxygen	O_2	1,429	1,105	-183,0	Oxidizing
Nitrogen	N_2	1,251	0,968	-195,8	Low reactive[c]
Hydrogen	H_2	0,090	0,070	-252,8	Reducing

[a] Specified at 0 °C and 0,101 MPa (1,013 bar).

[b] Sublimation temperature (solid to gas transition temperature).

[c] The behaviour of nitrogen varies with different materials and applications. Possible influences must be considered by the user.

According to AGA's handbook of shielding gases, a mixture gas can contain also other gases not listed in the standard. For instance, AGA's MISON® products contain nitrogen monoxide (NO). It is used to reduce the amount of ozone (O_3) produced by the burning arc, that is dangerous to welder's health. (AGA 1998, 8.) The amount of NO is relatively small, only 0.03 % of the mixture (AGA 1998, 54-57).

Mixture gases are typically compositions of two or three pure gases (table 2). Compositions of four are rare (excluding the aforementioned MISON® products). As can be seen from the table 2, there are over 30 groups and sub-groups available, each group specifying a range of mixture ratios. This leads in numerous possible mixtures. For example, AGA's handbook of shielding gases lists 23 different products (AGA 1998, 64-65).

TABLE 2. Gas mixture classification table (SFS-ISO EN 14175:2008)

Symbol		Components in nominal percentage of volume					
Main group	Sub-group	Oxidizing		Inert		Reducing	Low reactivity
		CO_2	O_2	Ar	He	H_2	N_2
I	1			100			
	2				100		
	3			balance	$0,5 \leq He \leq 95$		
M1	1	$0,5 \leq CO_2 \leq 5$		balance[a]		$0,5 \leq H_2 \leq 5$	
	2	$0,5 \leq CO_2 \leq 5$		balance[a]			
	3		$0,5 \leq O_2 \leq 3$	balance[a]			
	4	$0,5 \leq CO_2 \leq 5$	$0,5 \leq O_2 \leq 3$	balance[a]			
M2	0	$5 < CO_2 \leq 15$		balance[a]			
	1	$15 < CO_2 \leq 25$		balance[a]			
	2		$3 < O_2 \leq 10$	balance[a]			
	3	$0,5 \leq CO_2 \leq 5$	$3 < O_2 \leq 10$	balance[a]			
	4	$5 < CO_2 \leq 15$	$0,5 \leq O_2 \leq 3$	balance[a]			
	5	$5 < CO_2 \leq 15$	$3 < O_2 \leq 10$	balance[a]			
	6	$15 < CO_2 \leq 25$	$0,5 \leq O_2 \leq 3$	balance[a]			
	7	$15 < CO_2 \leq 25$	$3 < O_2 \leq 10$	balance[a]			
M3	1	$25 < CO_2 \leq 50$		balance[a]			
	2		$10 < O_2 \leq 15$	balance[a]			
	3	$25 < CO_2 \leq 50$	$2 < O_2 \leq 10$	balance[a]			
	4	$5 < CO_2 \leq 25$	$10 < O_2 \leq 15$	balance[a]			
	5	$25 < CO_2 \leq 50$	$10 < O_2 \leq 15$	balance[a]			
C	1	100					
	2	balance	$0,5 \leq O_2 \leq 30$				
R	1			balance[a]		$0,5 \leq H_2 \leq 15$	
	2			balance[a]		$15 \leq H_2 \leq 50$	
N	1						100
	2			balance[a]			$0,5 \leq N_2 \leq 5$
	3			balance[a]			$5 \leq N_2 \leq 50$
	4			balance[a]		$0,5 \leq H_2 \leq 10$	$0,5 \leq N_2 \leq 5$
	5					$0,5 \leq H_2 \leq 50$	balance
O	1		100				
Z	Gas mixtures containing components not listed, or mixtures outside the composition ranges listed.[b]						

[a] For the purpose of this classification, argon may be substituted partially or completely by helium.

[b] Two gas mixtures with the same Z-classification may not be interchangeable. <AC

2.2 Functional characteristics

The gas flow meter considered in this study is intended to be installed inside a welding wire feeder. Therefor the same requirements for functional characteristics of the welding gases apply on both the wire feeder and the gas flow meter. The requirements for the wire feeder are specified by several standards and specifications. In this study the functional characteristics include the following environmental and operational properties:

- gas temperature inside the gas flow meter,
- gas pressure inside the gas flow meter,
- flow rate minimum and maximum, and
- accuracy requirement for the flow rate.

Gas temperature inside the gas flow sensor can vary significantly. Kemppi welding equipment have limited operating temperature range from -20°C to +40°C (Kemppi 2016, 58). The heat effect of the welding current, the power consumption of the wire feeding motors, and the surrounding electronic components always increase temperatures inside a wire feeder during operation. It is assumed that during welding the temperature inside the wire feeder is always higher than the temperature outside. According to this assumption, the wire feeder never cools down the gas flowing through. Hence the lowest hypothetical limit for the gas temperature is -20°C. In cases where storage temperature has been below -20°C before welding, it is possible that a temporary cool down effect exists. These cases are extraneous and are out of the scope of this study.

Wire feeder's internal should never rise above the lowest value of maximum operating temperatures of certain components. In the case of this study wire feeder's microcontroller features the lowest maximum temperature of +85°C (NXP 2017, 40). This sets the highest hypothetical temperature for the gas to +85°C.

Due to the on/off manner of the gas flow during welding the temperature difference between the inner part of the wire feeder and its environment causes denoting gas temperature variation in the function of time. The effect of that variation has to be considered in this study.

Maximum gas pressure for welding wire feeders is specified in the standard IEC60974-5 and is 0.5 MPa (5 bar). This is the minimum requirement for the wire feeder parts being capable of operating without gas leakage. Under test conditions 0.75 MPa (7.5 bar) is applied for 30 seconds to proof that requirement. (IEC 2013, 11.) Based on common knowledge about gas support during welding, the gas pressure in the gas sensor varies depending on the following circumstances:

- gas support pressure (gas flow rate setup),
- the length of the torch cable set,
- inner diameter of the hose,
- cleanness of orifices in a gas nozzle, and
- possible bends in the hose.

A valve that controls the gas flow is regularly mounted inside the wire feeder before the gas flow sensor and other gas flow components and hoses. When the valve is closed, the remaining gas flows out from the gas nozzle and the gas pressure in the gas flow sensor becomes evened with the prevalent air pressure. When the valve is open, the pressure sets quickly on a level between 0.08 and 0.5 MPa, depending on the aforementioned circumstances. Higher pressures may exist, but they are erroneous and are not considered in this study. During operation the gas pressure does not vary from the achieved level significantly, if no sudden changes in the circumstances appear. The pressure difference between the flow and no-flow states has to be taken into account in this study.

Gas flow rate in the GMAW welding is set according to the shielding gas type, base material, welding current, arc type, gas nozzle size, torch orientation and desired draught. For steel, suitable flow rates vary from 10 l/min to 25 l/min in arc welding. These limits are referential. For example,

helium is less dense than argon and in aluminum welding the required flow rates of helium are multiple times higher than for argon. Both helium and argon are suitable for aluminum welding. (Lukkari 1997, 221.)

The flow value of 25 l/min is used in this study as the minimum requirement for the new gas flow sensor. Most calculations are performed by using 30 l/min as the upper limit. The table 3 lists the functional characteristics for welding gases in the welding environment and inside the welding system.

TABLE 3. Summary of the functional characteristics for welding gases

Characteristic	**Min**	**Max**
pressure	0.08 MPa	0.5 MPa
temperature (Celsius)	-20 °C	+85 °C
temperature (Kelvin)	253.15 K	358.15 K
flow rate	0 l/min	25 l/min

3 PHYSICAL PROPERTIES OF GASES

3.1 Intensive and extensive properties

In physics any characteristic of a system is called the property. The properties define the state of the system (Borgnakke & Sonntag 2009, 16). The properties can be divided into two categories, intensive and extensive properties. The intensive properties are independent of the size of the system, while the extensive properties depend on the extents of the system. The criterion to make difference between intensive and extensive properties is how the properties behave when the system is split in partial sub-systems. The intensive properties remain the same value on splitting. For example, the temperature of the sub-system is the same than the temperature of the whole system. The extensive properties get partial values when the system is divided into smaller parts. For example, the mass of the sub-system is less than the mass of the whole system. (Çengel & Boles 2015, 12.)

Some of intensive properties for gases are pressure, temperature, density and concentration, and some extensive properties are total volume and total mass (Çengel & Boles 2015, 12). Extensive properties per unit mass are called specific properties, and they behave as intensive properties (Borgnakke & Sonntag 2009, 16.) The table 4 lists the physical properties of gases examined in this study.

To examine properties of gas mixtures, the individual properties of each component in the mixture must be known. It is also necessary to know the rules about how certain individual properties form a mixture property when combined. There are different models, such as Dalton model of gas mixtures, which specify ways to combine gases within certain conditions (Borgnakke & Sonntag 2009, 466-467). Other models include but are not limited to Wilke mixture rule, Chapman-Enskog model, Wilke-Blottner-Eucken model and Stefan-Maxwell model. These models are beyond the scope of this study. Only the rules which are necessary in understanding the field of the gas mixture measurement are introduced.

TABLE 4. Intensive and extensive properties of gases

Property	**Symbol**	**Units**	**Extensive**	**Intensive**
density	ρ	kg/m^3		X
heat capacity (constant pressure)	C_p	J/K	X	
specific (molar) heat capacity (constant pressure)	c_p	$J/kg \times K$ $(J/mol\ K)$		X
heat capacity (constant volume)	C_v	J/K	X	
specific (molar) heat capacity (constant volume)	c_v	$J/kg \times K$ $(J/mol\ K)$		X
mass	m	kg	X	
pressure	p	Pa		X
temperature	T	K		X
thermal conductivity	k	$W/m \times K$		X
volume	V	m^3	X	
specific volume	v	m^3/kg		X
dynamic viscosity	η	$Pa \times s$		X
kinematic viscosity	γ	m^2/s		X
shear stress	τ	Pa		X
molar mass	M	kg/mol		X
volumetric flow rate	$\dot{V}$	l/s		X
mass flow rate	$\dot{m}$	$kg/s\ (g/s)$		X

3.2 Equations of state

According to Çengel and Cimbala, gas flow physics is not exact science. Laws and constants are based on large experimental data. Many phenomena can be explained by using an ideal-gas model. However, real gases differ more or less from that model. (2010, 322.)

Gas flow can be measured basically in two ways, by mass or by volume. Volumetric flow in liters per minute is commonly used to monitor the flow rate of the shielding gas in welding (Lukkari 1997, 189). The gas volume depends on pressure, temperature, a gas constant and the amount of gas. This is expressed in the ideal-gas equation of state:

$$pV = nR_mT \quad [1]$$

where p is pressure, V is volume, n is the molar amount of gas, R_m is the molar (universal) gas constant of $8.314510\ J/mol \times K$, and T is gas temperature in kelvin (Kuchling 1999, 248).

The specific (individual) gas constant R is different for each gas and is determined from

$$R = \frac{R_m}{M} \quad [2]$$

where M is the molar mass (also called the *molecular weight*) of the gas (Çengel & Cimbala 2010, 38).

By using the specific gas constant of a real gas, the equation of state can be written as

$$pV = ZmRT \quad [3]$$

where Z is the compressibility factor of the gas, and m is the actual mass of the gas (Çengel & Cimbala 2010, 306). The specific gas constants for the pure welding gases are listed in the table 5.

TABLE 5. Specific gas constants for pure welding gases (Kuchling 1999, 618)

Gas	$\boldsymbol{J/kg \times K}$
argon (Ar)	208
helium (He)	2078
carbon dioxide (CO_2)	188
oxygen (O_2)	260
nitrogen (N_2)	297
hydrogen (H_2)	4127

Based on the ideal gas equation of state, the volume of the gas in NTP (normal temperature and pressure) conditions is

$$V = nV_m \quad [4]$$

where V_m is the molar volume of the gas. By Avogadro's law the molar volume is almost constant for different gases in the same temperature and

pressure. For ideal gas it is $22.41410\ l/mol$ in STP (standard temperature and pressure) conditions. (Kuchling 1999, 247-248.)

Substance's mass is calculated from its molar amount and molar mass (Kuchling 1999, 247):

$$m = nM \quad [5]$$

Elements' molar masses can be read from the periodic table of elements. In molecular compounds the molar mass is the sum of compound's elements' molar masses. The table 6 lists molar masses of the pure gases and their elements.

TABLE 6. Molar masses of the pure gases and their elements from the periodic table of elements

Element	**Atomic mass** g/mol	**Gas**	**Molecular mass** g/mol
H	1.00794	H_2	2.01588
He	4.002602	He	4.002602
Ar	39.948	Ar	39.948
N	14.0067	N_2	28.0134
O	15.9994	O_2	31.9988
C	12.0107	CO_2	44.0095

The ideal gas model is applicable for certain gases, e.g. helium, near NTP conditions. For other gases and in different conditions the error of the ideal model increases. The real-gas equation of state is an approximation that works better for different gases in NTP conditions than the ideal-gas model. However, the real-gas model is inaccurate for gas mixtures. There

are other equations of state, for example van der Waals, Beattie-Bridgeman and Benedict-Webb-Rubin, that utilize more than one correction coefficients for better accuracy. (Çengel & Boles 2015, 141-143.)

The applicability of the ideal gas model can be estimated by the compressibility factor Z. For ideal gases the factor is 1, when for real gases it deviates from unity depending on temperature and pressure. The compressibility factor is relative to the critical point of the gas. It can be estimated by the means of Lee-Kesler simple fluid model (figure 2) that works especially for substances of simple molecules. (Borgnakke & Sonntag 2009, 64-65.)

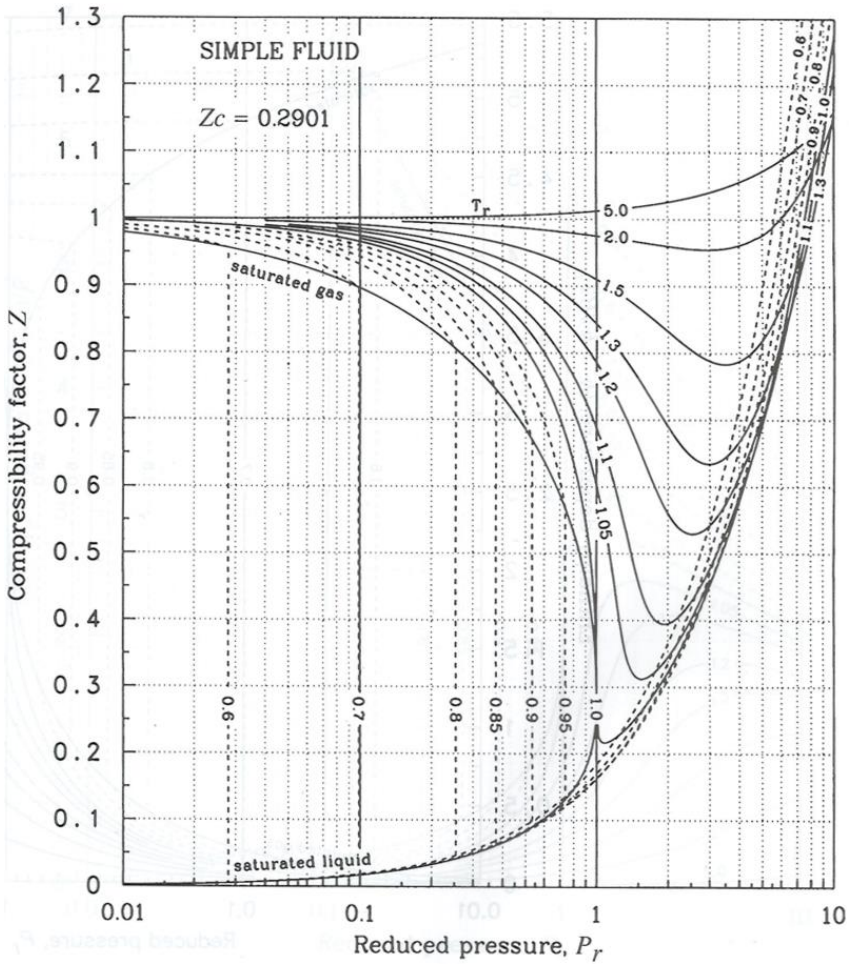

FIGURE 2. Lee-Kesler simple fluid compressibility factor (Borgnakke & Sonntag 2009, 755)

The simple fluid model is applied to a real gas by reducing its properties by the means of its critical point values:

$$P_r = \frac{P}{p_c} \quad [6]$$

$$T_r = \frac{T}{t_c} \quad [7]$$

where P_r is the reduced pressure, P is the pressure variable, and p_c is the pressure in the critical point. T_r, T and t_c are the counterparts for temperature. The critical temperature and pressure are the only parameters needed for use of the simple model where experimental data does not exist. (Borgnakke & Sonntag 2009, 65.)

The table 7 lists the critical point properties of the pure welding gases. As applied by the author, equations 6 and 7 for these gases result into the reduced temperature and pressure values listed in the table 8. Those values are calculated within the temperature and pressure limits of the welding environment's functional characteristics (table 3 on page 11). The table 9 represents the corresponding minimum and maximum values for the compressibility factor read from the Lee-Kesler simple fluid model. The minimum values are in minimum temperature and in maximum pressure (worst case), and the maximum values are in maximum temperature and in minimum pressure (best case).

TABLE 7. Critical properties (Borgnakke & Sonntag 2009, 684)

Gas	**Critical temperature** $t_c\ (K)$	**Critical pressure** $p_c\ (MPa)$
argon (Ar)	150.8	4.90
helium (He)	5.19	0.23
carbon dioxide (CO_2)	304.1	7.38
oxygen (O_2)	154.6	5.08
nitrogen (N_2)	126.2	3.39
hydrogen (H_2)	33.2	1.30

TABLE 8. Calculative reduced temperatures and pressures for the functional characteristics of the welding environment

Gas	T_r **min**	T_r **max**	P_r **min**	P_r **max**
argon (Ar)	1.679	2.375	0.016	0.102
helium (He)	48.775	69.006	0.348	2.174
carbon dioxide (CO_2)	0.832	1.178	0.011	0.068
oxygen (O_2)	1.637	2.317	0.016	0.098
nitrogen (N_2)	2.006	2.838	0.024	0.147
hydrogen (H_2)	7.625	10.787	0.062	0.385

TABLE 9. Approximate minimum and maximum compressibility factors for pure gases in welding environment according to the Lee-Kesler simple fluid model

Gas	Z_{min}	Z_{max}
argon (Ar)	1	1
helium (He)	1	1
carbon dioxide (CO_2)	0.97	1
oxygen (O_2)	0.95	1
nitrogen (N_2)	0.98	1
hydrogen (H_2)	1	1

In conclusion, the table 9 indicates ideal behavior for all gases in the minimum operating pressure and maximum temperature (Z_{max}). Carbon dioxide, oxygen and nitrogen deviate up to 5 % from the ideal gas behavior in the maximum pressure and minimum temperature (Z_{min}).

In this study the system is always considered to be static. This statement means that volume, temperature and pressure are always constants. Although volume, temperature and pressure can change in the function of time during operation, one and only one state may exist at the moment t of time. That assumption excludes enthalpy, entropy and other changes in the state of the system out of consideration. However, the equations of state are needed to calculate other properties like density or volume by mass.

3.3 Mass and mole fractions

The mixture ratio of welding gases is expressed as volumetric percentage of each pure gas component (SFS-EN ISO 14175 2008). The welding gases behave almost ideally in the conditions of the welding system (table 9 on page 20). Because the molar volume of the ideal gas is constant, the volumetric ratio is considered to be the same than the molar ratio in this study.

A mixture containing N components of pure gases has the total number of moles

$$n_{tot} = n_1 + n_2 + \cdots + n_N = \sum n_i \quad [8]$$

and the total mass, respectively:

$$m_{tot} = m_1 + m_2 + \cdots + m_N = \sum m_i \quad [9]$$

The mole fraction of each component is

$$y_i = \frac{n_i}{n_{tot}} \quad [10]$$

and concentration (mass fraction) of each component in the mixture is

$$c_i = \frac{m_i}{m_{tot}} \quad [11]$$

A mole basis can be converted to a mass basis by using the equation 5 on page 16:

$$c_i = \frac{m_i}{m_{tot}} = \frac{n_i M_i}{\sum n_j M_j} = \frac{n_i M_i / n_{tot}}{\sum n_j M_j / n_{tot}} = \frac{y_i M_i}{\sum y_j M_j} \quad [12]$$

and from the mass basis to the mole basis:

$$y_i = \frac{n_i}{n_{tot}} = \frac{m_i / M_i}{\sum m_j / M_j} = \frac{m_i / M_i m_{tot}}{\sum m_j / M_j m_{tot}} = \frac{c_i / M_i}{\sum c_j / M_j} \quad [13]$$

. (Borgnakke & Sonntag 2009, 464.)

4 KINEMATICS

4.1 Flow velocity and rate

Flow velocity is expressed in distance per time, for example m/s. The flow velocity in a tube is not uniform (Bohl 1998, 115). The velocity is practically expressed as an average value. The average velocity v is determined by volume V, time t, and cross-sectional area A of the tube (Kuchling 1999, 156):

$$v = \frac{V}{At} \quad [14]$$

The volumetric rate V/t is typically designated by symbol $\dot{V}$ (Kuchling 1999, 156; Bohl 1998, 116):

$$v = \frac{\dot{V}}{A} \Leftrightarrow \dot{V} = Av \quad [15]$$

The above equation can be expressed by the tube diameter d (Bohl 1998, 116):

$$v = \frac{\dot{V}}{\pi\left(\frac{d}{2}\right)^2} = \frac{4\dot{V}}{\pi d^2} \quad [16]$$

Mass flow rate $\dot{m}$ can be calculated from the volumetric flow rate by using density ρ:

$$\dot{m} = \rho A v = \rho \dot{V} \quad [17]$$

4.2 Viscosity

Internal friction (toughness) of a fluid influences an object moving in the fluid, or the fluid moving on walls. The coefficient of the friction is called the *dynamic viscosity* η. The SI unit of the dynamic viscosity is Pascal seconds ($Pa \times s$). The quotient of the dynamic viscosity and the density of the fluid is called the *kinematic viscosity* γ:

$$\gamma = \frac{\eta}{\rho} \quad [18]$$

(Kuchling 1999, 162-163.) The dynamic viscosity increases when temperature increases. Sutherland correlation for the dynamic viscosity for gases as a function of temperature is expressed as

$$\eta = \frac{aT^{1/2}}{1 + \frac{b}{T}} \quad [19]$$

where T is absolute temperature and a and b are constants that are determined experimentally (Çengel & Cimbala 2010, 49). The table 10 represents the kinematic and dynamic viscosities for the pure gases in STP conditions.

TABLE 10. Dynamic and kinematic viscosities (Kuchling 1999, 611-612)

Gas (in 0°C, 1013 hPa)	$\boldsymbol{\eta}$ $(\mu \boldsymbol{Pa} * \boldsymbol{s})$	$\boldsymbol{\gamma}$ $(\boldsymbol{mm2/s})$
argon (Ar)	21.2	11.9
helium (He)	18.7	105
carbon dioxide (CO_2)	13.7	6.93
oxygen (O_2)	19.2	13.4
nitrogen (N_2)	16.5	13.2
hydrogen (H_2)	8.42	93.7

Viscosity in a mixture can be estimated by using variety of equations. A typical approach is to calculate sum of partial viscosities by summing the products of the viscosities of the pure gases and their mole fractions:

$$\eta_{mix} = \sum_i (x_i \times \eta_i) \quad [20]$$

By Thomas Davidson, this model is adequate for mixtures of components with similar molecular weights. For components with different molecular weights this model deviates significantly. Other partial viscosity models, like introduced by Wilke, Golubev and Schmick, contribute experimental correction coefficients. More accurate models are viscosity of interaction by Chapman and Cowling, and the simple and accurate method to calculate viscosity for gaseous mixtures by Davidson himself. (Davidson 1993, 2.)

Although there are different methods to calculate the viscosity of a mixture more or less accurately, the most important thing in this study is to understand the contribution of different component's viscosities in the mixture. From the sum of partial viscosities (equation 20) can be derived that the viscosity of the mixture can never be higher than its most viscous component or less than its least viscous component (figure 3).

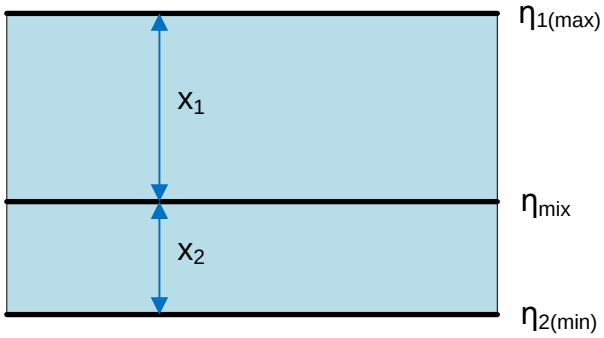

FIGURE 3. Partial sum of viscosities of a mixture

4.3 Turbulence and laminarity

In laminar flow, fluid particles move parallel to a streamline without mixing with each other (figure 4). In turbulent flow, they continuously move traverse to the flow transport axis (figure 6). There is a region between the turbulent and laminar flow where the flow is transitional (figure 5). (Bohl 1998, 115-116.)

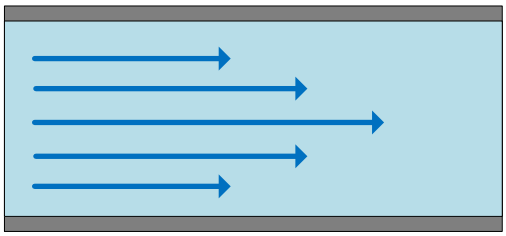

FIGURE 4. Laminar flow

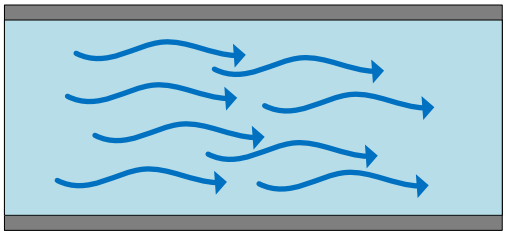

FIGURE 5. Transitional flow

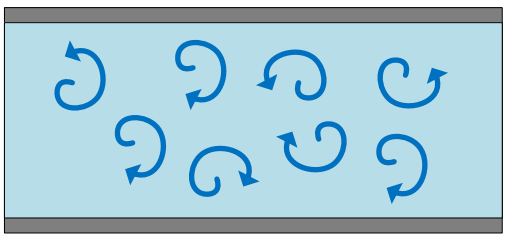

FIGURE 6. Turbulent flow

The flow characteristics can be determined by Reynolds number Re. It is a dimensionless quantity that describes inertial and viscous forces in different flow conditions. Large experimental data has revealed that for laminar flow in a tube an approximate value $Re_{crit} \approx 2320$ is critical: values $Re < Re_{crit}$ represent laminar flow when values $Re > Re_{crit}$ represent transitional or turbulent flow (Holman 2010, 217; Bohl 1998, 116). By Kuchling the critical value is $Re_{crit} \approx 1160$ (1999, 169), but this appears to be a mistake in comparison with other sources. By Holman a hysteresis range of $2000 \leq Re \leq 4000$ is generally accepted to use for transitional flow (2010, 217), while others claim the range to be $2320 \leq Re \leq 4000$. The variation between the sources emphasizes the experimental nature of the Reynolds number.

The Reynolds number can be calculated by using several equations. An equation suitable for flow in small tubes is

$$Re = \frac{v * d}{\gamma} \qquad [21]$$

where v is average flow velocity, d is tube diameter and γ is kinematic viscosity. According to the equation, an increase in velocity and in tube diameter increase the Reynolds number, while increase in kinematic viscosity decreases it. That is, in small tubes and with low velocities the flow is laminar more likely than in large tubes and/or high velocities. (Bohl 1998, 112-114.)

4.4 Entry length

When a uniform-velocity flow of a fluid enters a circular tube, it starts developing. The development is caused by frictional forces between the flowing fluid and the surface of the tube. The flow layer in contact with the surface stops, and slows down the adjacent layer. The effect of the friction continues to slow down other layers towards the center of the tube. Near the entrance the flow is irrotational and develops until it achieves a parabolic velocity gradient. After achieved, the gradient does not change until the tube diameter changes. The region of the tube where flow development takes place is called the entrance region. It is followed by a fully developed region (figure 7). (Çengel & Cimbala 2010, 325.)

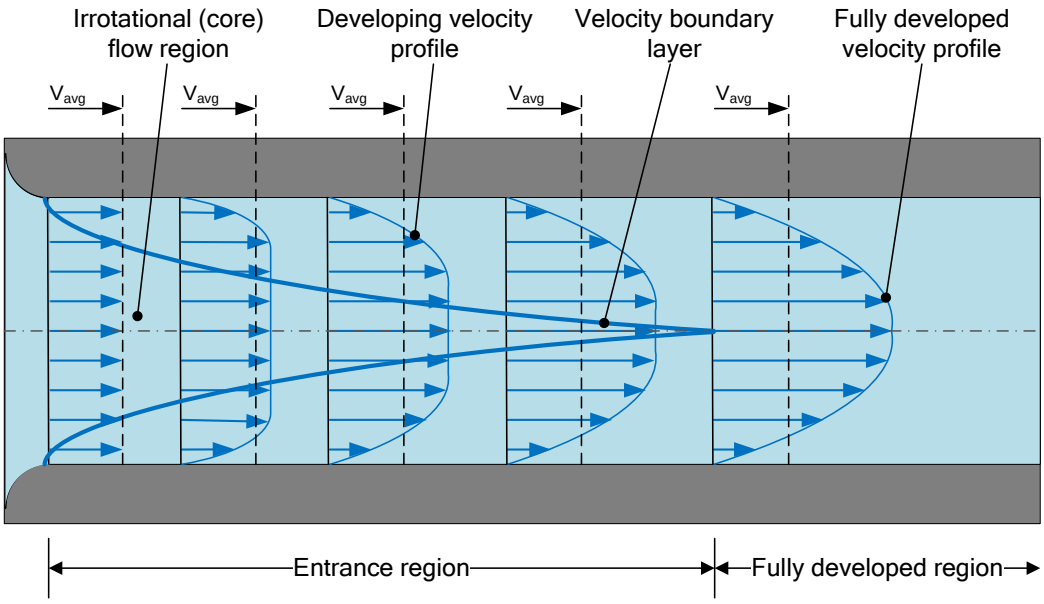

FIGURE 7. Flow development in a tube

The length of the entrance region is called the entry length. The entry length depends on the flow velocity. For Reynolds number $Re = 20$ it is the size of the diameter. For the critical number $Re = 2300$ it is $115D$ (115 times the diameter). For turbulent flow the entry length can be approximated as

$$L_h = 1.359 D Re_D^{1/4} \quad [22]$$

and the dependency on the Reynolds number is less significant. This results into much shorter entry length for turbulent flow than for laminar flow. Practically the entrance effects become insignificant when the pipe length is 10 times the diameter:

$$L_h \approx 10D \quad [23]$$

This length applies also when the flow is turbulent at the entrance of the tube, but the Reynolds number in the tube is less than 2300. (Çengel & Cimbala 2010, 326-327.)

5 THERMODYNAMICS

5.1 Specific heat capacities and degrees of freedom

Heat is energy in transit. Heat added to a substance increases kinetic energy of molecules. In point-like (monatomic) gases energy is stored into three-dimensional (translational) motion of the particle (figure 8). For ideal gas of point particles in constant volume, the specific heat capacity C_v is

$$C_v = \frac{3}{2} R_m \qquad [24]$$

where R_m is the universal gas constant and the number 3 the number of velocity components in translational motion. The number of the velocity components is called *degrees of freedom*. (Young & Freedman 2012, 605.)

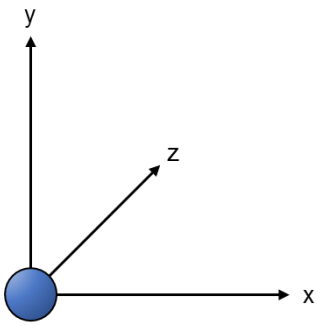

FIGURE 8. Translational degrees of freedom

When the molecule has more than one atoms, energy is stored in additional velocity components. Diatomic molecules store energy in two rotational components (figure 9). Rotation around diatomic molecule's longitudinal axis does not account because energy of that axis does not transfer between molecules in collisions. This applies also to simple

polyatomic molecules where atoms are in line, for example carbon dioxide (figure 10). For complex polyatomic gases all three rotational degrees of freedom contribute in heat capacity (figure 11). (Young & Freedman 2012, 606.)

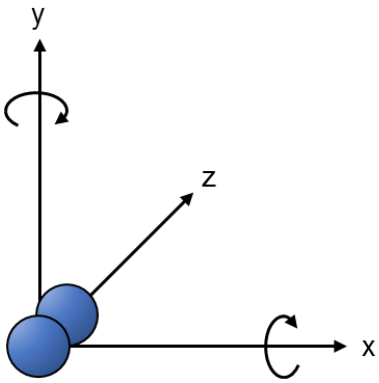

FIGURE 9. Rotational degrees of freedom of a diatomic molecule

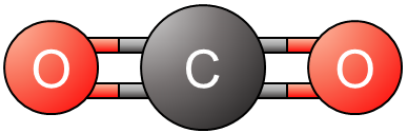

FIGURE 10. Linear geometry of a CO_2 molecule

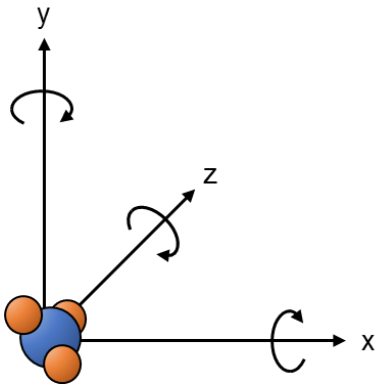

FIGURE 11. Rotational degrees of freedom of a polyatomic molecule

Molecular bonds can behave like springs, storing additional energy into vibration (figure 12). This vibration increases the degrees of freedom (Demtröder 2015, 270). In solid substances molecules are not able to move or rotate, and the vibration is the only storage for heat energy (table 11). For the most diatomic and polyatomic gases, the vibration normally does not contribute to heat capacity, but starts to count when temperature increases, involving some concepts of *quantum mechanics* (figure 13) (Young & Freedman 2012, 606).

FIGURE 12. Vibration of a polyatomic molecule

In addition to the string-like vibration, in polyatomic molecules also other dimensions of vibration, called bending, contribute to heat capacity. Kuchling's table of degrees of freedom (table 11) does not take vibration or bending into account. The total degrees of freedom depend on the number of atoms in the molecule as well as the geometry of the molecule, as explained in the table 12.

TABLE 11. Degrees of freedom by Kuchling (Kuchling 1999, 306)

Substance	**Translation**	**Rotation**	**Vibration**	**Sum**
1-atomic gas	3	-	-	3
2-atomic gas	3	2	-	5
3-atomic gas (*)	3	3	-	6
Solids			6	6

(*) CO_2 behaves like a diatomic gas

TABLE 12. Degrees of freedom, a universal table

Substance	Translation	Rotation	Vibration	Total
Monatomic gas	3	0	0	3
Linear molecules	3	2	3N-5	3N
Nonlinear molecules	3	3	3N-6	3N

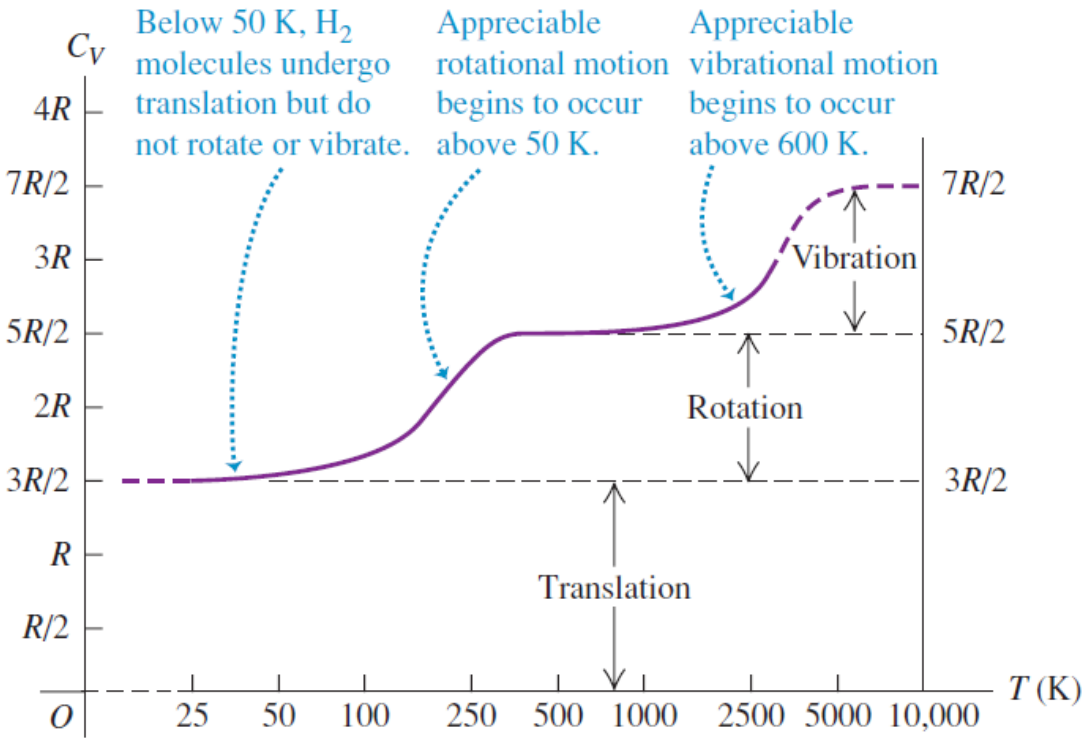

FIGURE 13. The molar heat capacity of diatomic hydrogen gas in the function of temperature (Young & Freedman 2012, 607)

The amount of kinetic energy in each velocity component is explained by the principle of equipartition theorem, derived from statistical mechanics. By the principle, the kinetic energy of a molecule per velocity component is

$$\frac{1}{2}kT \qquad [25]$$

where k is the Boltzmann constant and T the temperature in kelvin. To contribute each velocity component, the equation 25 is multiplied by 3 for monatomic gases, by 5 for diatomic gases and by 6 for polyatomic gases. (Young & Freedman 2012, 606.) The molar isochoric (constant volume) heat capacity is thus

$$C_v = \frac{1}{2}f_{eff} \times R_m \qquad [26]$$

where f_{eff} is the effective amount of degrees of freedom in the particular state of the system (Demtröder 2015, 270).

The isochoric heat capacity is smaller than isobaric (constant pressure) specific heat capacity. In isobaric process the volume expands, and the work of expansion consumes heat energy. The difference between the isobaric and isochoric heat capacities is

$$C_p = C_v + R_m \qquad [27]$$

Deploying that into the equation 26 gives

$$C_p = \frac{1}{2} \times (f + 2)R_m \qquad [28]$$

The ratio between the isobaric and isochoric specific heat is expressed as

$$\kappa = \frac{C_p}{C_v} = \frac{f+2}{f} \qquad [29]$$

and is called the *adiabatic index.* (Demtröder 2015, 269.)

National Institute of Standards and Technology Joint Army-Navy-NASA-Air Force (JANNAF) Interagency Propulsion Committee (NIST-JANAF) provides tables for isobaric molar specific heats of gases in the function of temperature (NIST-JANAF 2017). The figure 14 represents those values in a logarithmic-scale diagram for the pure welding gases.

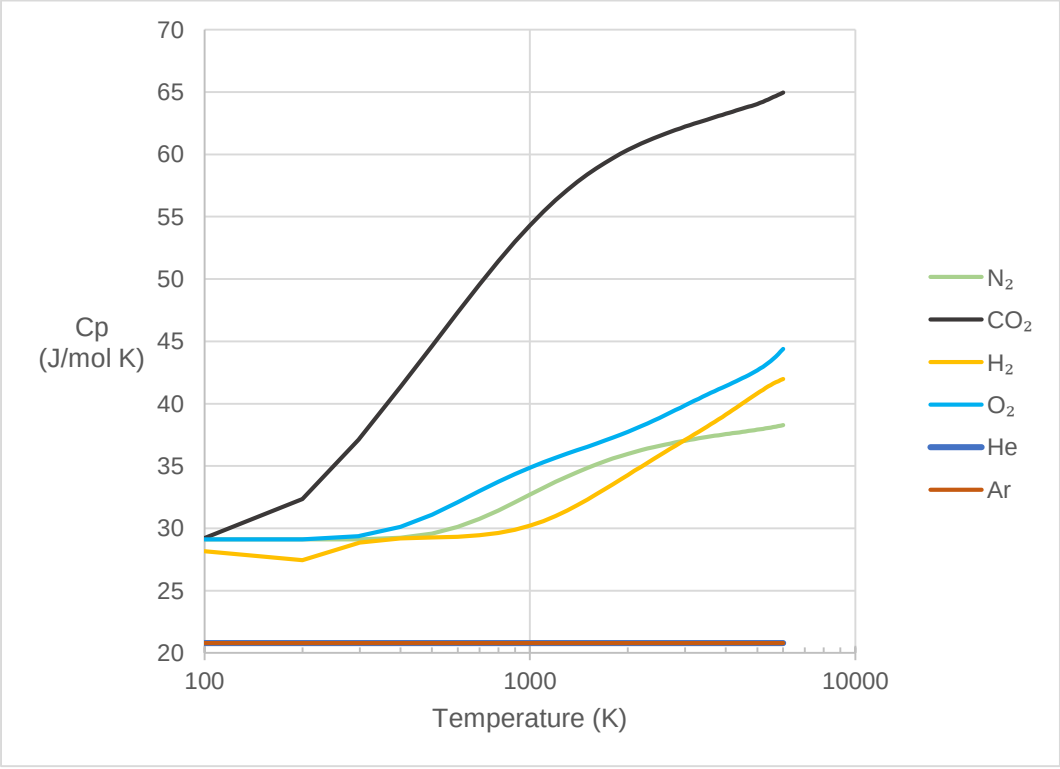

FIGURE 14. Isobaric molar heat capacities of pure welding gases (NIST-JANAF 2017)

Based on the equation 28 on page 34, degrees of freedom can be calculated from the isobaric molar heat capacities as

$$C_p = \frac{1}{2} \times (f + 2) R_m \iff f = \frac{2C_p}{R_m} - 2 \qquad [30]$$

that produces a diagram shown in the figure 15. The vertical dash lines represent the temperature range of the welding environment.

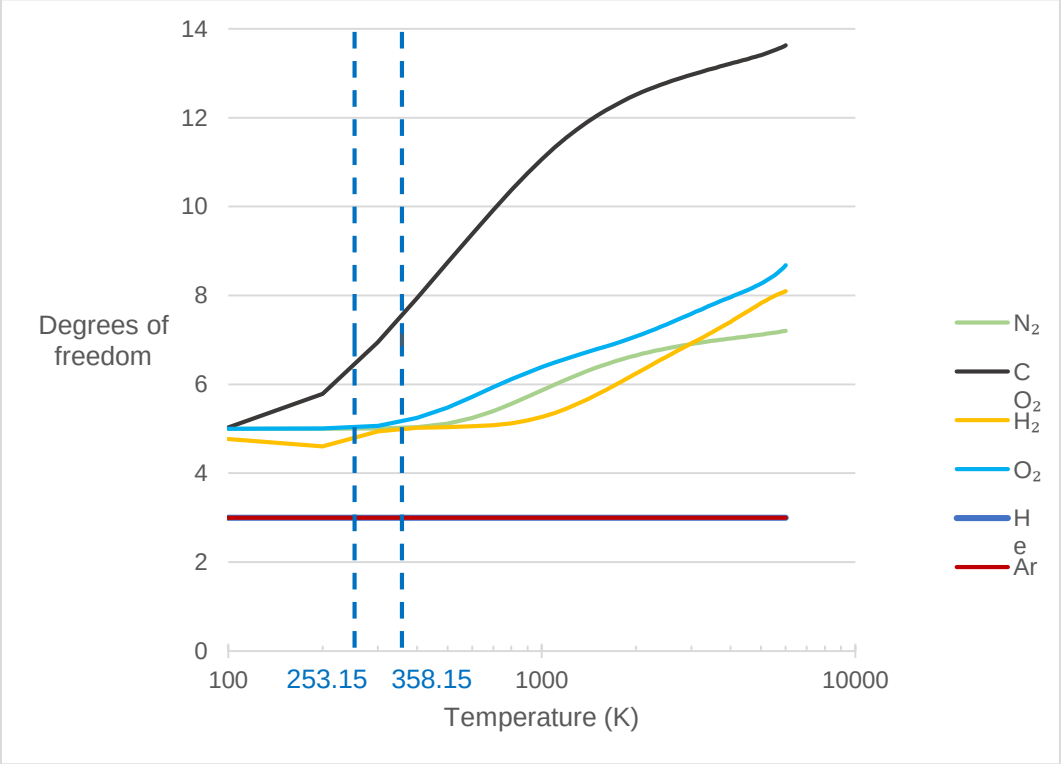

FIGURE 15. Degrees of freedom for pure welding gases according to the NIST-JANAF isobaric molar heat capacities

The figure 16 represents the degrees of freedom in a linear scale diagram from the range of interest. Noble gases argon and helium have three degrees of freedom throughout the range. Diatomic gases follow the assumption of five degrees of freedom in the room temperature almost

linearly in the range of interest. However, the estimated five degrees of freedom for carbon dioxide in the room temperature, due to molecule's linear geometry, does not match with the experimental data. The conclusion is that vibrating and bending degrees of freedom begin to contribute in the heat capacity of carbon dioxide in relatively low temperatures. This anomaly is caused by heaviness of the atoms of the CO2 molecule and can be explained by the equipartition theorem. The explanation is beyond the scope of this study.

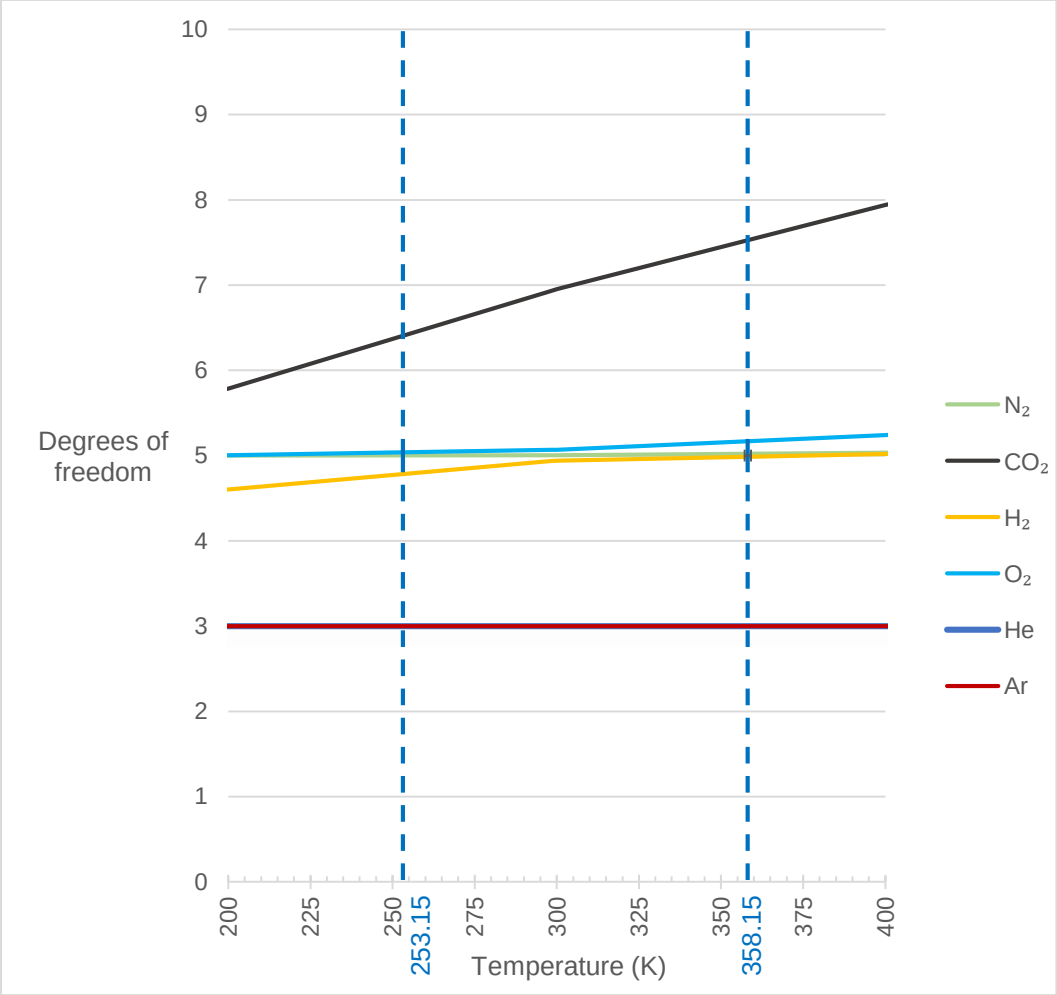

FIGURE 16. Degrees of freedom of the pure welding gases within the temperature range of the welding system

5.2 Conductive heat transfer

Conduction is energy transfer from a surface to a surrounding bulk. The conduction takes place with solid materials as well as with fluids. In gases heat is transferred (conducted) in collisions of gas molecules. (Holman 2010, 5-6.)

Fourier's law of conduction is expressed as:

$$\dot{Q}_{cond} = -k_t A \frac{dT}{dx} \quad [31]$$

where dx is the constant thickness of the layer, k_t is the thermal conductivity of the layer material (solid or fluid), A is the surface area normal to the direction of heat transfer and dT is temperature difference between the surfaces of the layer (figure 17). (Çengel & Boles 2015, 91.)

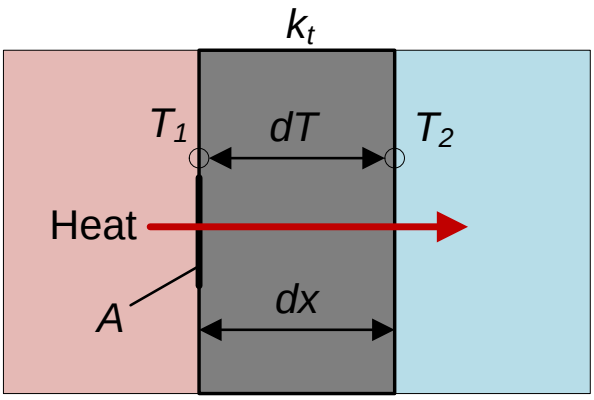

FIGURE 17. Conductive heat transfer

5.3 Convective heat transfer

Convection is energy transfer from a solid surface by combination of *conduction* and *fluid motion*. The convection can be free (natural) or forced. The forced convection means that the flow is forced by a fan, a pump or another source while in natural convection the fluid motion is generated by a heat gradient in the fluid. (Çengel & Boles 2015, 92.) In welding the shielding gas flow is forced by the pressure of the gas container.

By Newton's law of cooling, the heat transfer rate by convection is

$$\dot{Q}_{conv} = hA\left(T_s - T_f\right) \quad [32]$$

where h is the convection heat transfer coefficient, A is the area of the surface, T_s is the surface temperature, and T_f is the fluid temperature before the surface. The convection can be expressed also in the function of time:

$$\dot{Q}_{conv} = hAt\Delta T \quad [33]$$

(Kuchling 1999, 315). The convection heat transfer coefficient h is an experimental value that combines all environmental properties, such as gas velocity, gas properties, the nature of gas motion, surface geometry etc. Typical values for the h in forced convection of gases are in the range of $25 - 250\, W/m^2K$. (Çengel & Boles 2015, 93; Borgnakke & Sonntag 99.)

6 GAS FLOW METERING

6.1 Gas flow measurement techniques

Gas flow can be measured in many ways, each way having specific applications. In welding the gas flow rate is typically reported in liters per minute (volumetric flow). Another way to report gas flow is in mass units per time (mass flow).

Andrew Mangell's article about flow measurement techniques in World Pumps Magazine discusses about strengths and limitations of the current gas flowmeter technology. Mangell compares together Coriolis, differential pressure, positive displacement, thermal, turbine, ultrasonic, variable area and vortex flowmeter techniques. He partly disagrees with flow control experts about distinguish between 'new' and 'old' technology; he prefers technologies suitable for use in digitalized systems as 'new'. By Mangell, these are thermal, Coriolis, ultrasonic and vortex techniques. (2008.)

According to Mangell, the best practice to measure gases and steam is to measure mass flow. This is because volumetric flow rates do vary with temperature and pressure changes significantly, affecting to the accuracy and repeatability. From the preceding four techniques, Coriolis and thermal techniques measure mass flow when ultrasonic and vortex techniques measure velocity of the gas. Multiplying velocity by tube's cross-sectional area gives volumetric flow as the result. (2008, 34.)

6.2 Thermal mass flow sensing

The history of thermal mass flow sensing is relatively short. According to an article published in SVC Summer Bulletin 2010, one of the earliest thermal sensors was introduced in 1911. It is called Thomas flow meter by the inventor C. C. Thomas and was based on a heater and two temperature sensors in a tube (figure 18). Different solutions to measure mass flow by heating the substance were Laub flow meter (figure 19) introduced by J. H. Laub in 1947 and Benson flow meter (figure 20) introduced by J. M. Benson in 1965. (Alvesteffer et. al. 2010, 42-43.)

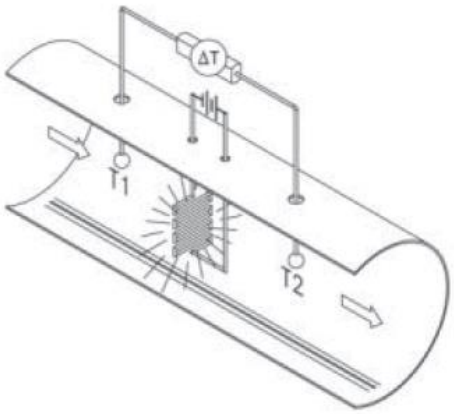

FIGURE 18. Thomas flow meter (Alvesteffer et. al. 2010, 42)

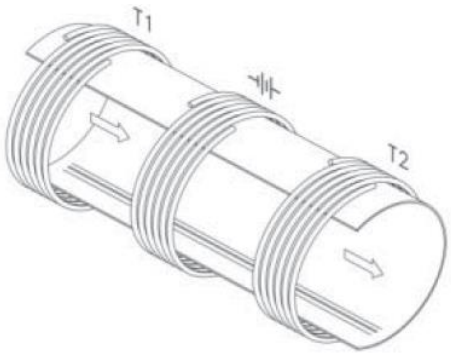

FIGURE 19. Laub flow meter (Alvesteffer et. al. 2010, 42)

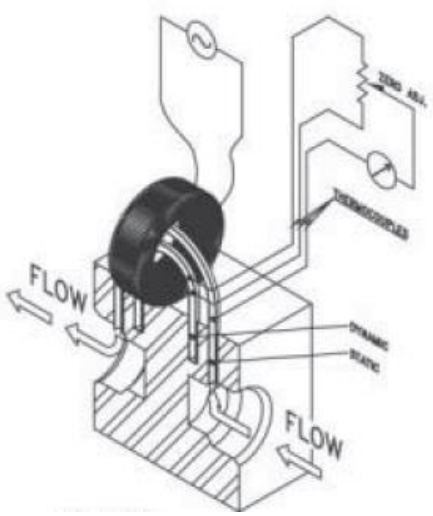

FIGURE 20. Benson flow meter (Alvesteffer et. al. 2010, 43)

The figures 18, 19 and 20 show that Thomas flow meter, Laub flow meter and Benson flow meter all require complex construction according to their mechanical structure and the amount of key components. Complexity usually increases the cost of the device.

6.3 Constant temperature anemometry

One way to measure gas flow thermally is to use a hot-wire anemometer. One application of the hot-wire anemometer is a constant temperature anemometer (CTA). It consists of three key components: a hot-wire probe, a Wheatstone bridge and a servo amplifier (figure 21). (Dantec Dynamics 2017.) By Dantec, constant temperature anemometry is particularly suitable for examination of flow characteristics in turbulent flows. However, the Swiss sensor manufacturer Innovative Sensor Technology IST AG states the CTA being suitable for mass flow measurement equally in both laminar and turbulent flow (IST AG 2016c, 4).

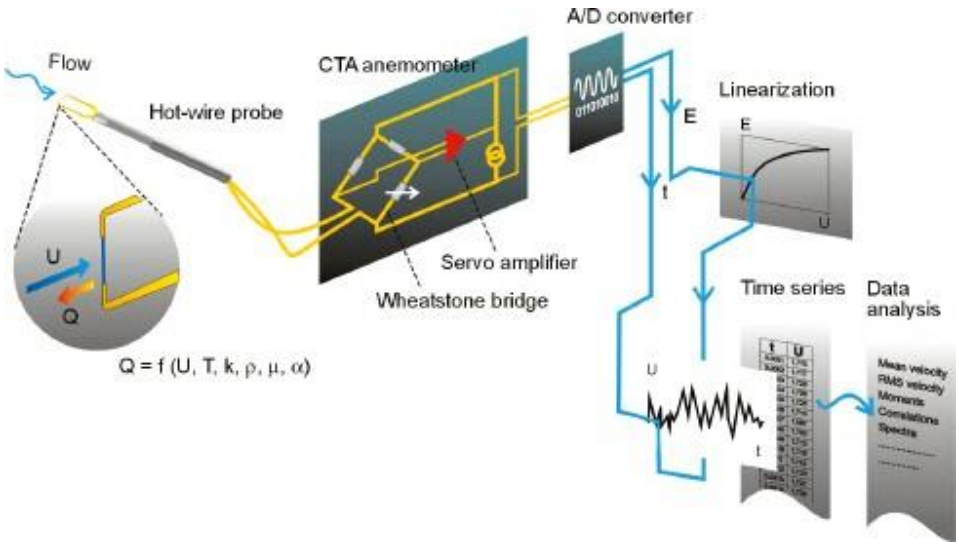

FIGURE 21. The principle of the hot-wire anemometer (Dantec Dynamics 2017)

The Wheatstone bridge is a resistor network that is commonly used to determine the value of an unknown resistance. It is named by Sir Charles Wheatstone who popularized it in 1840s. The Wheatstone bridge consists of two series-parallel resistor arrangements that are connected between a voltage supply and ground (figure 22). When balanced, it produces zero voltage difference between the two parallel branches C and D. (ElectronicsTutorials 2017.)

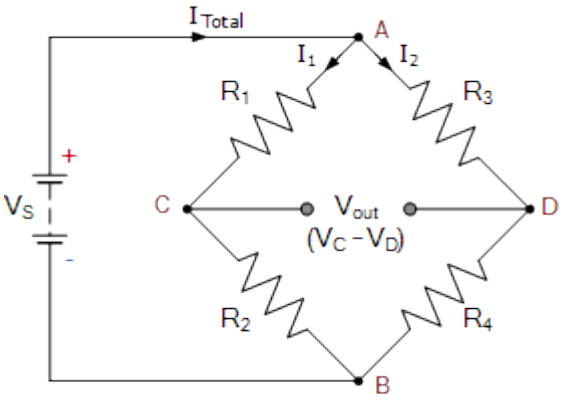

FIGURE 22. Typical illustration of the Wheatstone bridge (ElectronicsTutorials 2017)

In the most basic CTA circuitry one resistor of the Wheatstone bridge is replaced by a hot-wire probe. Parallel branches C and D are connected to an operational amplifier that controls the voltage over the bridge. The bridge is balanced by the other three resistors so that in zero-flow condition the probe is on a certain level of temperature above the temperature of the measured fluid. The basic CTA circuit fits in applications where the temperature of the fluid never reaches the temperature of the hot-wire probe. In advanced CTAs the fluid temperature is compensated by replacing another resistor of the Wheatstone bridge by a temperature sensing resistor (figure 23). This resistor together with an offset resistor keeps the difference between probe's and fluid's temperatures constant. (IST 2016c, 2.)

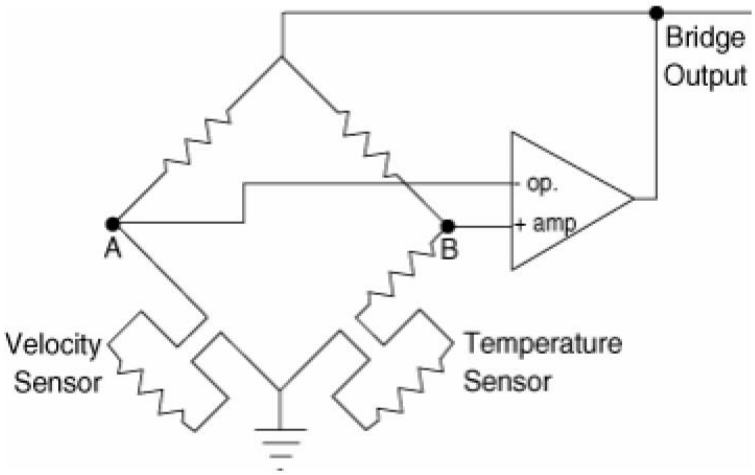

FIGURE 23. CTA connection diagram with temperature compensation (IST 2016c, 2)

Flowing fluid cools down the hot-wire probe by the forced convection affecting the resistance of the hot wire. When resistance changes, the bridge goes out of balance. The operational amplifier reacts to the unbalanced state and increases the voltage over the bridge to maintain the balance. Increase in voltage increases power dissipation of the hot-wire probe increasing its temperature and resistance, and the bridge

becomes balanced again. The voltage U over the bridge in the function of the flow rate $\dot{V}$ (figure 24) is well described by the King's law:

$$\dot{V} = (T_w - T_0)A_w h = A + BU^n, n \approx 0.3..0.5 \quad [34]$$

where $T_w - T_0$ is the wire over-temperature and the physical properties of the fluid, A_w is the wire surface area and h the heat transfer coefficient. These are merged into the calibration constants A and B. (Dantec Dynamics 2017.)

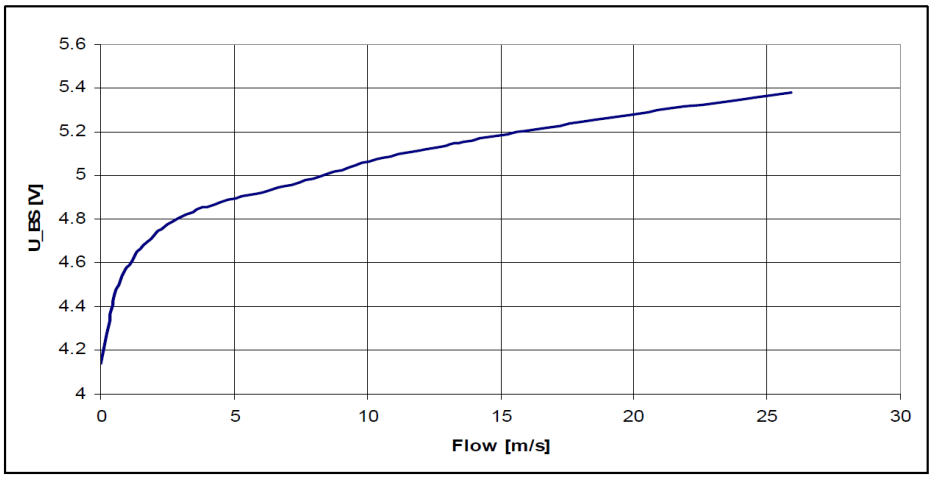

FIGURE 24. Typical output of the CTA bridge (IST AG 2016b)

7 APPLIED STUDY

7.1 Sensor selection

An FS5 thermal mass flow sensor, manufactured by IST, had been previously used by Kemppi in a gas flow indicator product. The sensor had been selected because of its simplicity, robustness and accuracy. The sensor was made of a ceramic plate with two platinum PTC (positive temperature coefficient) type resistors, heater and reference, etched on it. Although it had benefits, there were also disadvantages experienced with this product: the sensor had unacceptably long 2-minute warm-up time and 2-second response time.

IST suggested using an FS2T sensor as a replacement for the FS5. It had less than 30-second warm-up time and 0.5-second response time. The new sensor had two additional resistors for flow direction detection (figure 25). Because of the additional resistors, there were also additional wires in the sensor: the FS2T had total of six wires (table 13) when the FS5 had only three wires.

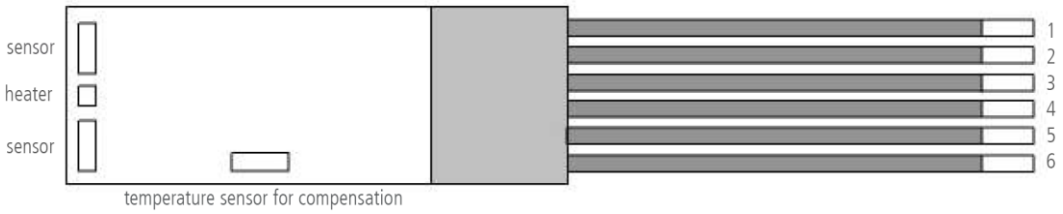

FIGURE 25. Layout of the FS2T sensor (IST AG 2016b)

TABLE 13. FS2T wiring (IST AG 2016b)

Wire number	**Function**
1	GND (common to the temperature sensors)
2	Temperature sensor (left)
3	Heater
4	Heater
5	Temperature sensor (right)
6	Temperature sensor (reference)

The table 14 lists the key properties of the FS2T sensor. In evaluation tests the sensor was found faster and more accurate than the FS5 sensor.

TABLE 14. Properties of the FS2T sensor (IST AG 2016b)

Property	**Value**
Accuracy	< 2 % of the measured value
Response time	< 0.5 s
Operating temperature range	-20 °C to +150 °C
Heater	R_H (25 °C) = 34 Ω ±10 %
Reference element	R_S (25 °C) = 34 Ω ±10 %
Voltage range (nominal)	2 V to 5 V

The FS2T sensor element had not got a housing available in the IST product catalogue. Based on the existing housing of the FS5, the new housing and the overall mechanical construction was specified in co-operation with IST. Because the direction detection was not needed in this product, the amount of wires coming out from the housing was decreased to four by letting the wires 2 and 5 unutilized. The figure 26 is an illustration about the final construction of the sensor component.

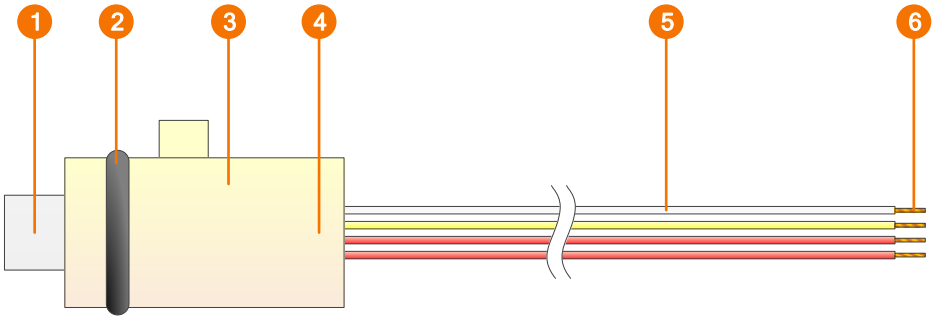

1 FS2T sensor element
2 O-ring
3 Hot-melt housing
4 Wire extension inside the housing
5 Stranded wires
6 Stripped and coated wire endings

FIGURE 26. The final construction of the FS2T sensor component in the specification

7.2 Mechanical prototyping

The evaluation of the thermal mass flow sensor FS2T was started from a mechanical construction that had been designed for Kemppi's existing gas flow indicator product. That product had been equipped with a preceding version of IST's sensor model, FS5. The measures of the new flow tube were copied from that product. Sensor's fixing hole was enlarged for the FS2T sensor that was physically bigger than the FS5 sensor. The first prototype had a 3.5 mm diameter straight tube with relatively low 60 mm overall length, and the sensor was mounted middle of the tube (figure 27).

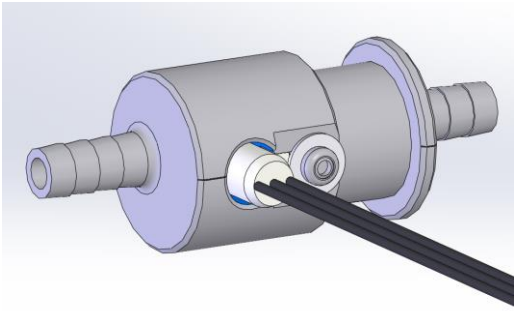

FIGURE 27. The first prototype with a 3.5 mm flow tube

The mechanical part was CNC-machined from a bar of polyoxymethylene (POM), also known as polyacetal. That material was recommended to the author of this study for machining feasibility, low cost, and sufficient stability in different conditions.

The gas velocity for the maximum volumetric flow of 30 l/min in the 3.5 mm tube was calculated by using the velocity equation 16 introduced on page 23. Units were converted from liters to cubic meters, from millimeters to meters and from minutes to seconds:

$$v = \frac{4\dot{V}}{\pi d^2} = \frac{4 \times \frac{0.03m^3}{60s}}{\pi \times 0.0035^2 m^2} \approx \underline{51.97\, m/s} \qquad [35]$$

Maximum applicable velocity in CTA mode for the FS2T was 100 m/s according to sensor's datasheet (IST AG 2016b, 1). Thus the calculated velocity in the 3.5 mm tube was within that boundary. However, this design resulted in low ADC (analog-to-digital conversion) resolution for CTA output voltage on high velocities as seen in the following diagram (figure 28). The formation of the graph in that diagram is analogous with sensor's datasheet (IST AG 2016b, 5).

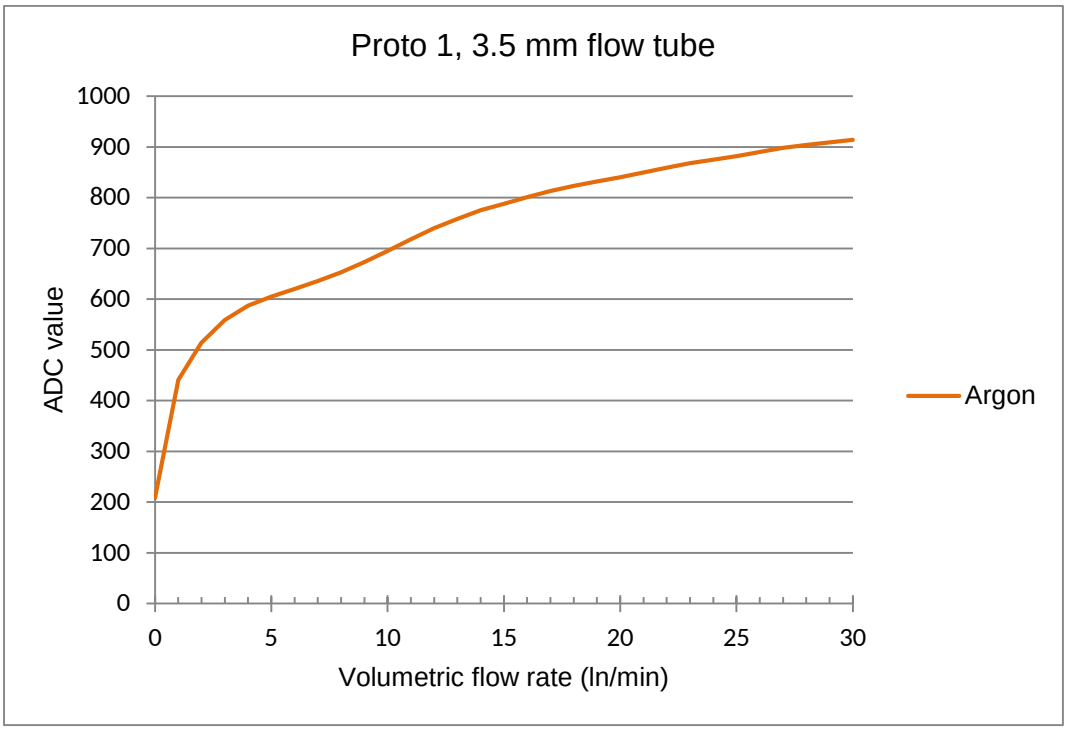

FIGURE 28. ADC values in the function of norm-volumetric flow for argon in a 3.5 mm flow tube

Lower resolution in ADC values would lead in decreased accuracy with converted flow rate values. As seen in the precedent diagram, there are approximately 60 ADC steps between 20 l/min and 30 l/min. That results in 6 steps/l, or 0.17 l/step. In comparison, there are 73 steps/l or 0.014 l/step in between 1 l/min and 2 l/min.

To achieve better accuracy for CTA output values, the maximum flow velocities were calculated for different sizes of tubes (figure 29). Based on the calculations, 8 mm diameter was selected for the next prototype. With that size the maximum flow velocity would be 9.95 m/s, which locates to the beginning of the almost-linear high-resolution section of the flow curve.

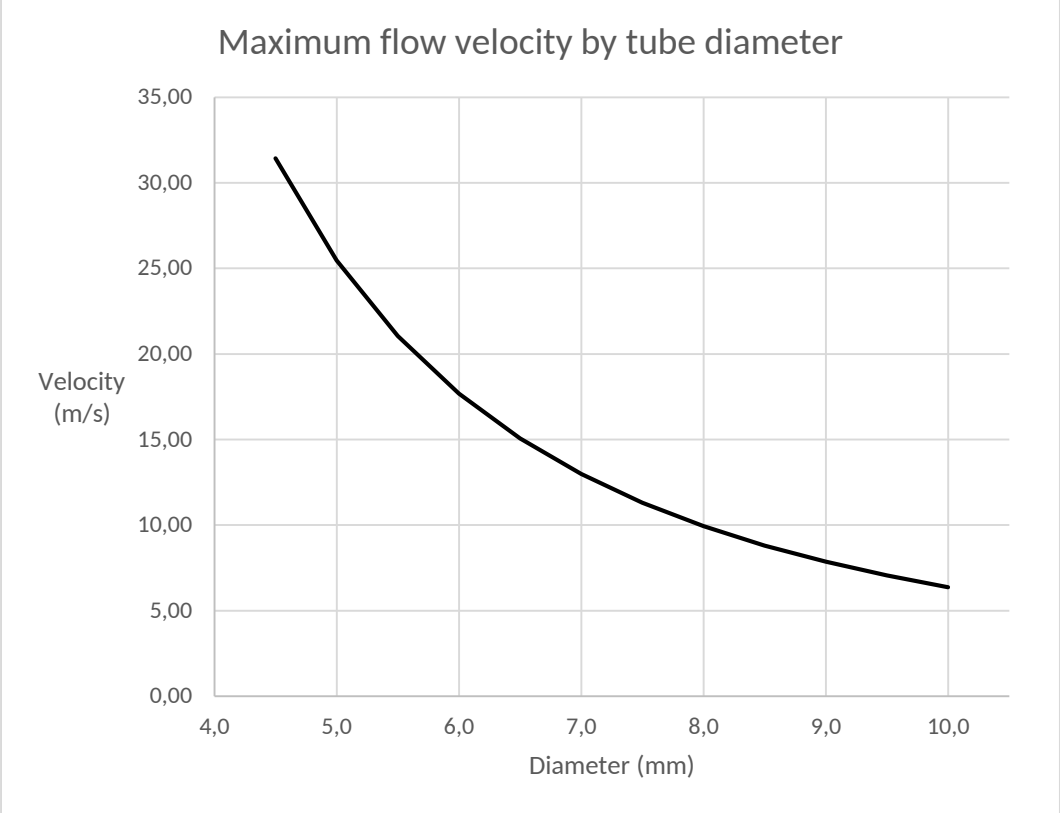

FIGURE 29. Maximum flow velocities for different tube sizes at 30 l/min flow rate

The second prototype was CNC-machined from a POM bar like the first one (figure 30). In the beginning of the flow tube, there was a tooled hose-coupling with 3.5 mm inner diameter. The 8 mm measurement tube was drilled from the other end through the part. The FS2T sensor was located 60 mm from the entry side of the 8 mm part of the flow tube. In the other end there was a thread for a brass-metal hose-coupling.

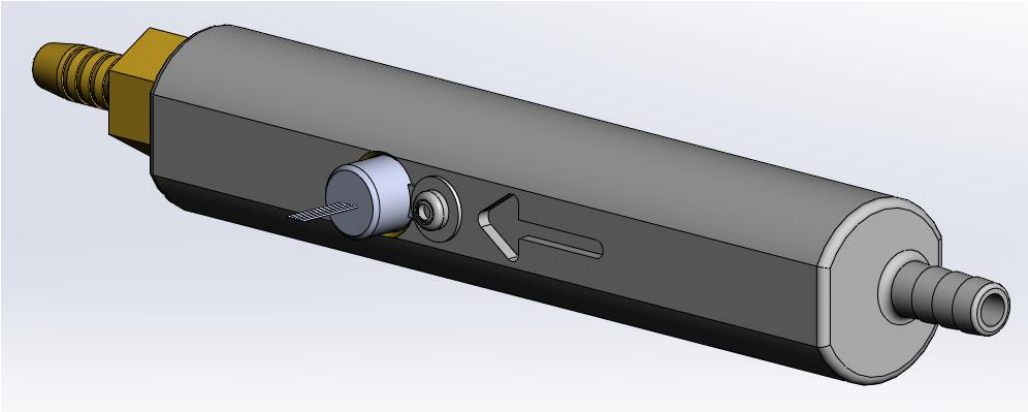

FIGURE 30. The second prototype with 8 mm flow tube

Measurements with the second prototype showed increased accuracy for argon. The measurements were performed also with a mixture of 82 % argon and 18 % carbon dioxide, and the results were promising (figure 31). Flow rates below 2.0 l/min indicated an inconsistent peak in ADC values, which caused flow rates below 3.5 l/min to be unpredictable for both gases.

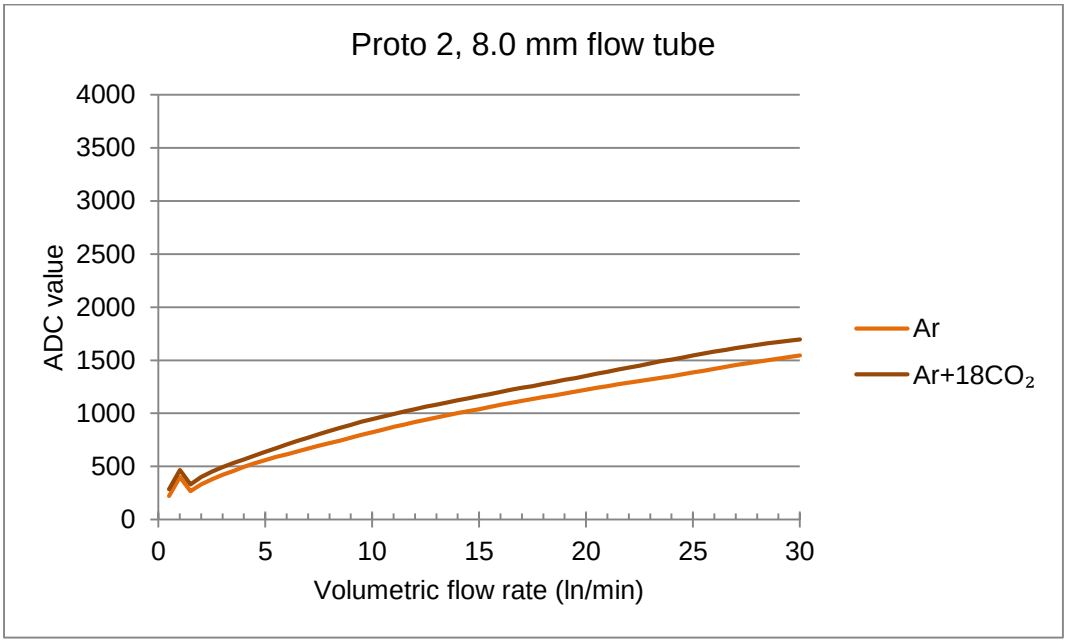

FIGURE 31. ADC values in function of volumetric flow for argon and argon / carbon dioxide mixture in an 8.0 mm flow tube

The measurements were continued for pure carbon dioxide and helium gases. As seen from the diagram (figure 32), the helium graph indicated significant inconsistence causing values less than 26.0 l/min being unreliable, when the carbon dioxide was less aware of this phenomenon. That required further investigation on the flow mechanics.

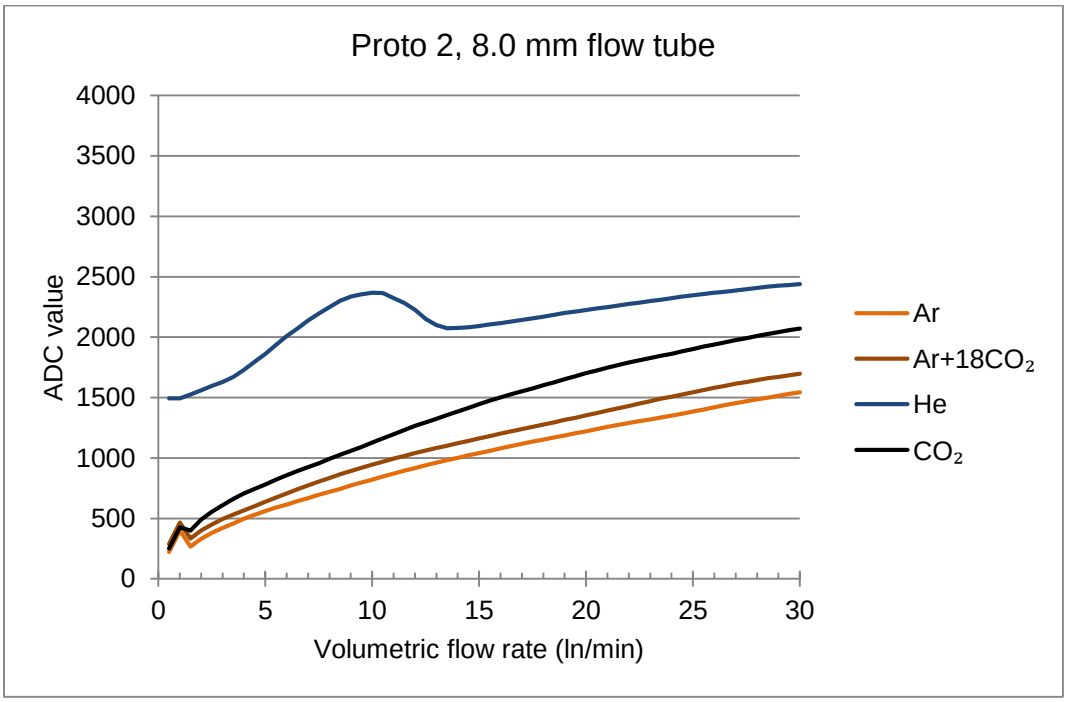

FIGURE 32. Second measurements for the 8.0 mm flow tube

It was noticed that the inconsistency of helium was explained by the theory of laminar and turbulent flow. By calculating Reynolds number for the 8.0 mm tube it could be seen that helium and hydrogen were never turbulent in the range of observation, while other gases became turbulent with relatively low flow values (table 15). Transient flow is highlighted in yellow and turbulent flow in red color in the table.

TABLE 15. Reynolds numbers for pure gases in 8.0 mm tube

l/min	Ar	He	CO_2	O_2	N_2	H_2
5	1115	126	1914	990	1005	142
10	2229	253	3828	1980	2010	283
15	3344	379	5742	2969	3014	425
20	4458	505	7655	3959	4019	566
25	5573	632	9569	4949	5024	708
30	6687	758	11483	5939	6029	849

A comparison between the Reynolds numbers calculated for the first and second prototypes showed that in the 3.5 mm tube the measured gases were practically always in turbulent motion (table 16). This explained why there was no sign of inconsistency for argon in the first prototype.

TABLE 16. Reynolds numbers for pure gases in 3.5 mm tube

l/min	Ar	He	CO_2	O_2	N_2	H_2
5	2547	289	4374	2262	2297	324
10	5095	577	8749	4525	4593	647
15	7642	866	13123	6787	6890	971
20	10190	1155	17498	9049	9186	1294
25	12737	1444	21872	11312	11483	1618
30	15285	1732	26247	13574	13780	1941

To achieve the best measurement results in all conditions of interest, the laminar flow was set to a target of this study. The entrance length found affecting to the length of the flow tube, so its diameter had to be as small as possible. The minimum size was 3.5 mm with the FS2T sensor, as in the first prototype. But as experienced in the first prototype, a small tube would lead to a high velocity. A quick prototype with a small-diameter measurement tube and a larger diameter bypass tube was built to solve this issue (figure 33). The bypass tube would reduce the flow velocity in the measurement tube.

FIGURE 33. Evaluation prototype of the bypass tube

By a brief evaluation, the concept of the bypass tube seemed to be applicable. However, it was necessary to investigate more on the flow behavior in different constructions before making a new prototype. A mechanical designer was consulted by the author of this study to find out a construction that would be suitable for mass production. One aim was to keep the external size of the mechanical part so small that it could be machined from a 30 mm diameter POM bar. The resulted construction included two 7.5 mm bypass channels with a 4.0 mm measurement tube.

The third prototype (figure 34) was made by using these measures. Reynolds numbers were calculated to an array (table 17) and are represented as a diagram in the figure 35.

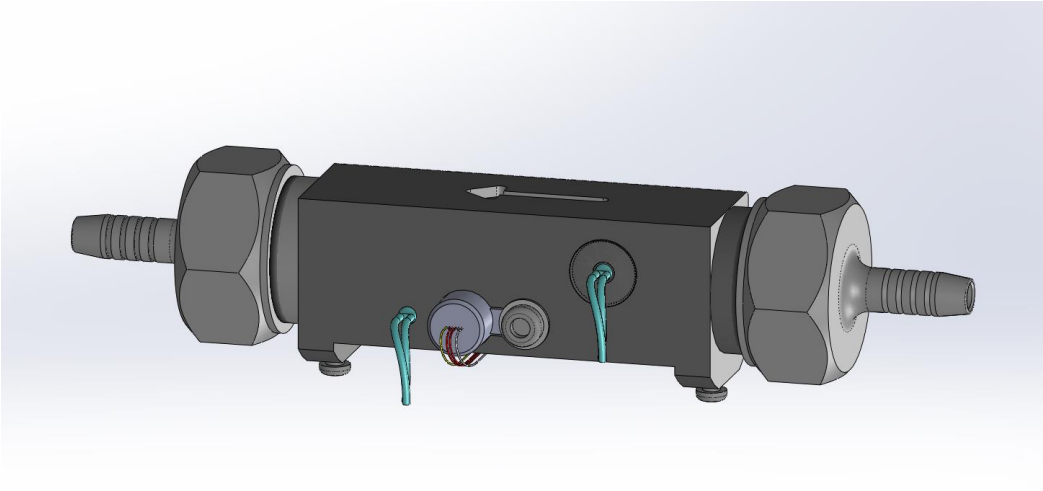

FIGURE 34. The third prototype with a 4 mm flow tube and two 7.5 mm bypass channels

TABLE 17. Reynolds numbers for 4 mm measurement tube with two 7.5 mm bypasses

l/min	**Ar**	**He**	**CO_2**	**O_2**	**N_2**	**H_2**
5	278	31	477	246	250	35
10	555	63	953	493	500	70
15	833	94	1430	739	751	106
20	1110	126	1906	986	1001	141
25	1388	157	2383	1232	1251	176
30	1665	189	2860	1479	1501	211

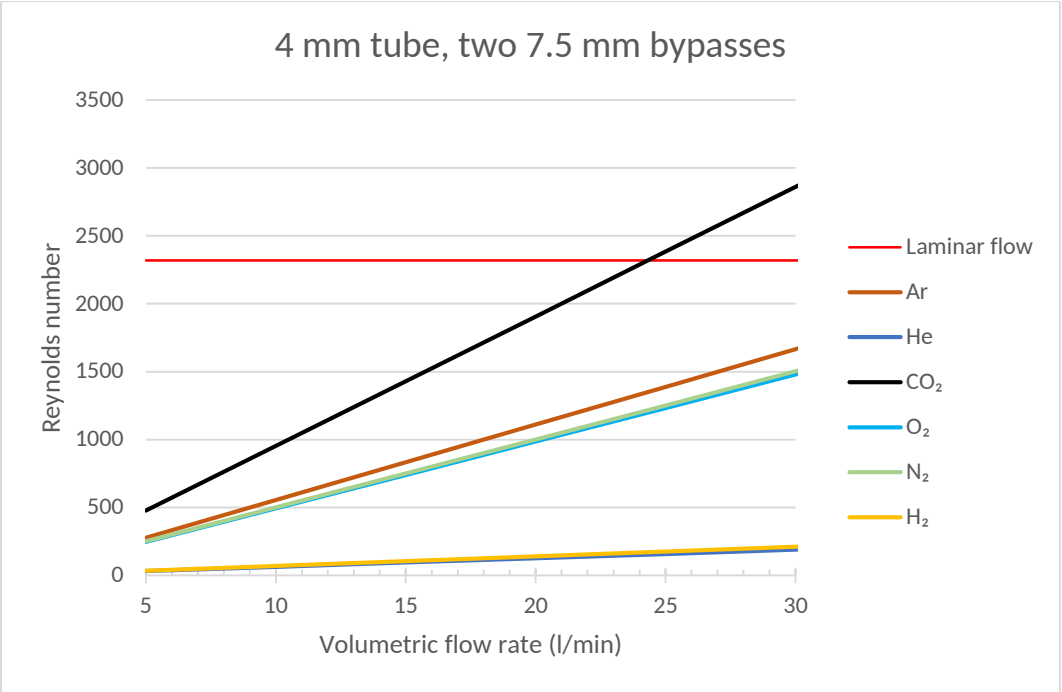

FIGURE 35. Graphs for Reynolds numbers of table 17

When compared with the previous investigations on the two prototypes, this design gave much better results. However, carbon dioxide was still an issue. It entered to the transitional region with flow rates just above 25 l/min.

Reynolds numbers in previous calculations were calculated in NTP conditions. The situation would become worse with lower than 0°C temperatures and higher than 1 bar pressures. This fact together with the previous calculations forced to think alternative constructions. There was no room for larger bypass channels, and calculations for the minimum 3.5 mm size of the measurement tube did not help enough. Therefor an orifice plate was decided to be used in the design. The equation was modified and Reynolds numbers calculated with different orifice sizes. A 1.5 mm orifice gave very good results without reducing flow rate too much (table 18). The values are represented in a new diagram (figure 36).

TABLE 18. Reynolds numbers for 4 mm measurement tube with two 7.5 mm bypasses and 1.5 mm orifice plate

l/min	Ar	He	CO_2	O_2	N_2	H_2
5	44	5	75	39	39	6
10	87	10	150	78	79	11
15	131	15	225	116	118	17
20	175	20	300	155	158	22
25	219	25	375	194	197	28
30	262	30	450	233	236	33

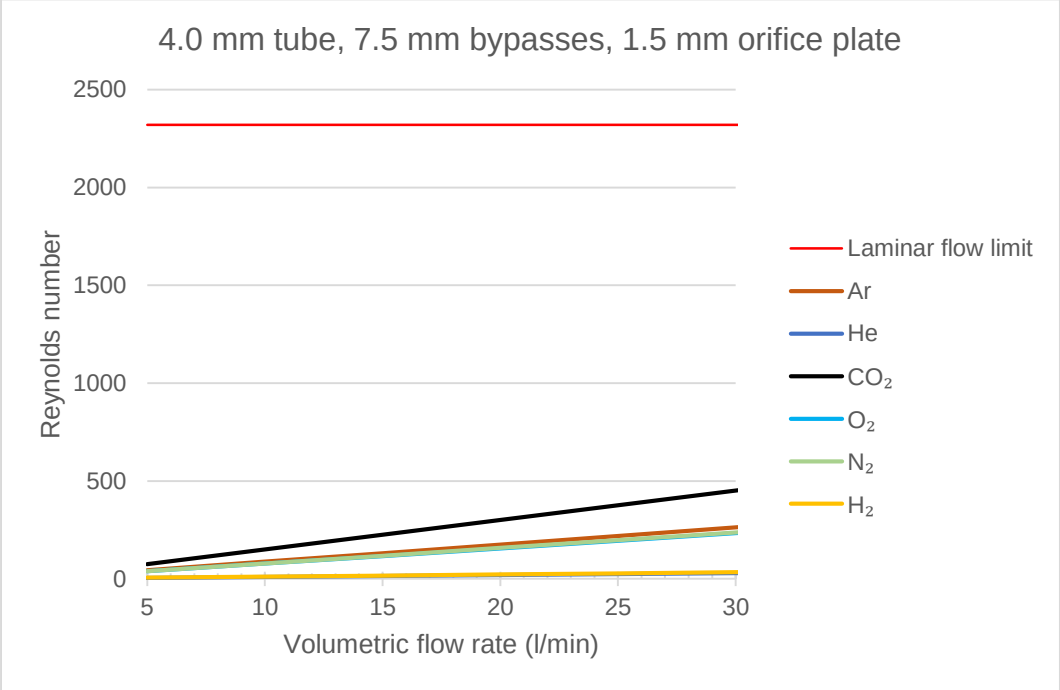

FIGURE 36. Diagram for Reynolds numbers of table 18

Different ways to implement the orifice plate compared in co-operation with a mechanical designer. Key questions were manufacturing suitability, part availability and the structure of the flow tube element. A 5 mm long nylon tube choke with 1.5 mm inner diameter was found applicable instead of the orifice plate in the beginning of the 4.0 mm measurement tube. This did not change tube element's functional properties significantly.

Brief measurements with the third prototype showed that there was a balancing issue with the three tubes. The flow balance between the measurement tube and the bypass tubes varied by the flow rate. To solve this issue, a sintered-metal porous filter was added to the input chamber of the element. Furthermore, two temperature sensors were added for temperature compensation, one to a bypass channel and another near the flow sensor. The construction of the third prototype is illustrated in the figure 37. The figure 38 represents the cross section of the third prototype.

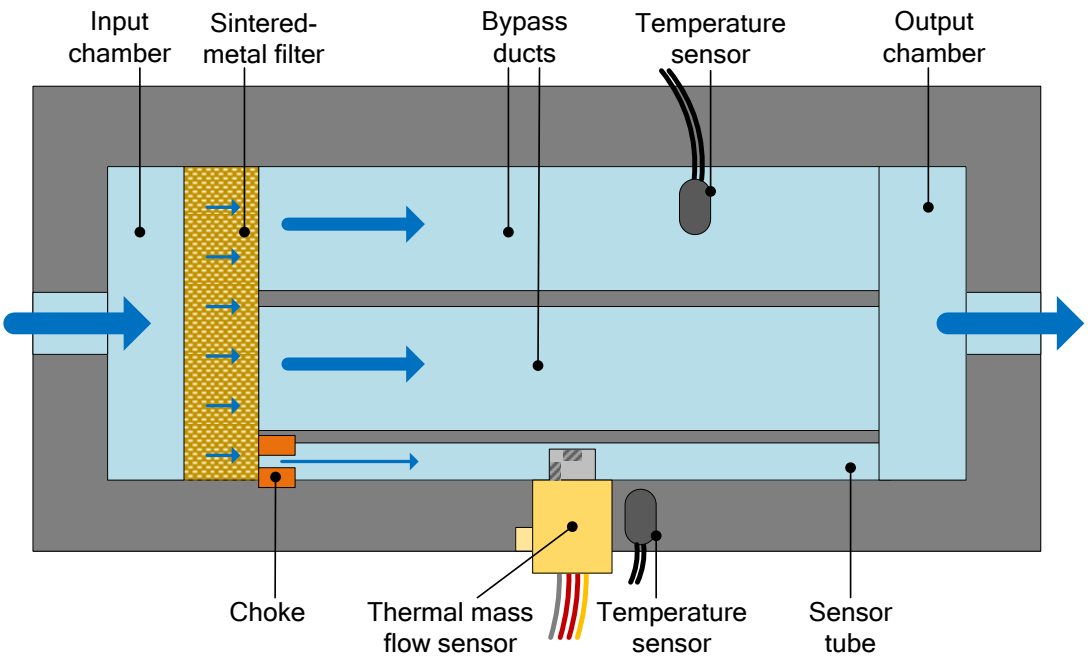

FIGURE 37. Functional drawing of the third prototype

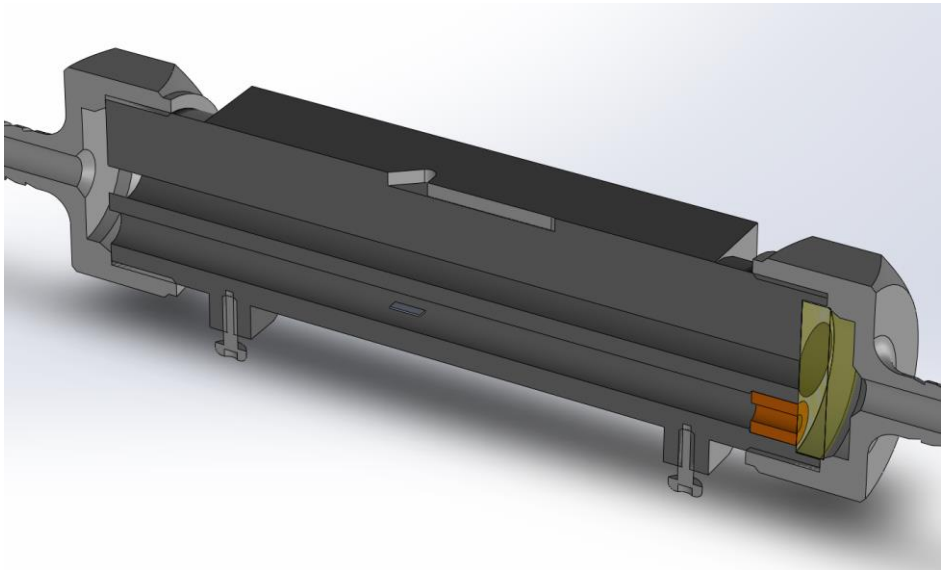

FIGURE 38. Cross-section of the third prototype

In the third prototype, gas entered from a hose to the input chamber, where it got equally distributed to bypass channels and to the sensor tube by the sintered-metal filter. The filter also divided gas flow into small adjacent layers within the tubes for smoother entrance. After flow tubes the gas entered the output chamber and exit to a hose.

Measurements with the third prototype indicated that the gas flow was laminar within the whole flow range for each measured gas. The measurements where made with helium that is the second lightest of the welding gases, carbon dioxide that is the heaviest, and argon that has the lowest heat transfer rate. The velocity in the measurement tube was at low-flow range and the resolution of the characteristic curves was applicable (figure 39). Based on these facts the third mechanical prototype was decided to be used in the final product.

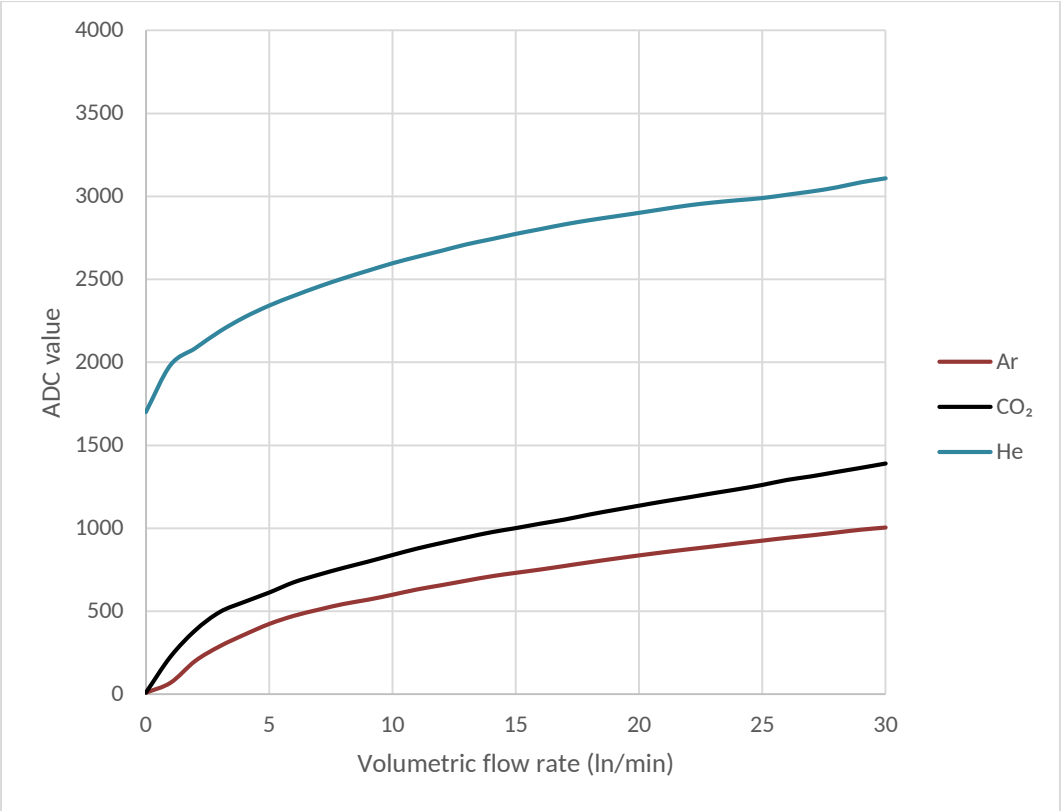

FIGURE 39. Characteristic curves for argon, carbon dioxide and helium measured with the third prototype

7.3 Hardware prototyping

The first version of the FS2T sensor driver was based on the design of the existing gas flow detector product with a potentiometer-adjustable CTA bridge. The potentiometer was replaced with the PWM (pulse-width modulation) controlled analogue switch *Q2* that drove the resistor *R6* in series with the resistor *R1* (figure 40). The output of the CTA bridge was scaled into the range of MCU's (micro-controller unit) A/D (analog-to-digital) converter by the operational amplifier *U1* and filtered by a low-pass filter (figure 41).

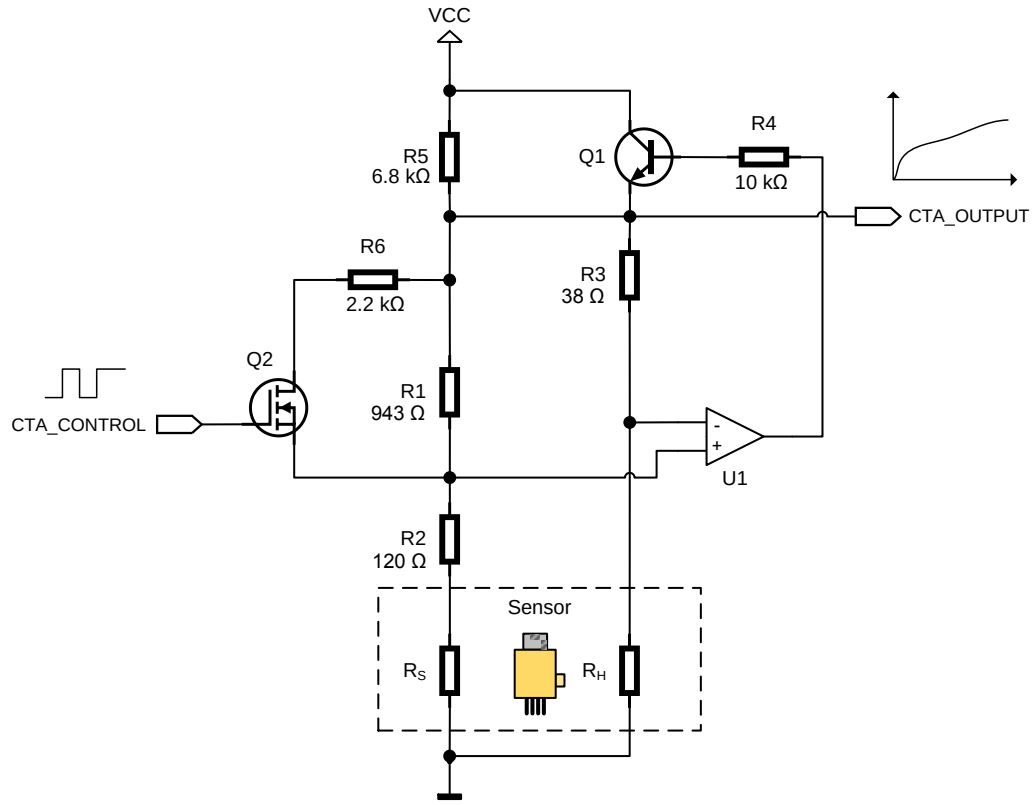

FIGURE 40. The first prototype of the CTA bridge

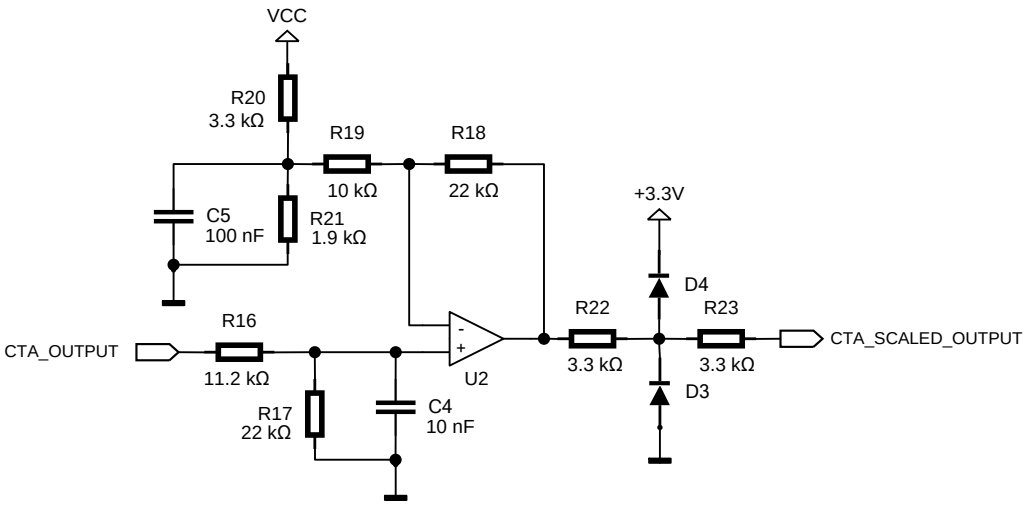

FIGURE 41. Output scaling and filtering circuitry

The first prototype was calibrated by the means of the *CTA_CONTROL* signal by adjusting the *CTA_OUTPUT* to a constant voltage value in zero-flow conditions, to a so-called zero-flow point. After setting the zero-flow point, the gas flow was measured in two fixed flow points of 10 l/min and 20 l/min, and compared the measured values to a pre-measured characteristic curve. If they differed too much from the curve, the calibration was judged a failure.

This version of CTA was able to measure gas flow rates accurately in constant temperature conditions. However, further measurements quickly divulged the circuit very sensitive to changes in gas temperature. That made measured gas flow rates unreliable.

Investigations on the IST application note (2016a, 2) revealed that the first attempt for CTA calibration methodology was defective. The resistor *R2* that set the temperature offset between the heater R_H and the gas temperature should have been replaced by a short-circuit for calibration. Then, the output of the operational amplifier *U1* should have been adjusted to its lowest value to achieve balance on the bridge. Balancing the bridge would have improved its resistivity to gas temperature variations. In the second prototype, the CTA circuitry modified by adding FETs (field-effect transistor) *Q3* and *Q4* to enable on/off control of the offset resistor *R2* (figure 42).

In laboratory tests an additional issue appeared: when applying full power over the CTA bridge during calibration, the heater R_H was activated. This had not been taken into account in the IST application note. That caused heater's resistance to change due to increasing temperature, affecting negatively to the bridge balance. The bridge balance could be managed only when the bridge driver transistor *Q1* was disabled. In that case, the bridge was powered by quiescent current through the pull-up resistor *R5*. A new FET *Q5* was added to enable bridge on/off control. For simpler layout with reduced amount of assistive components, the Wheatstone bridge was flipped upside down and the sensor placed in the upper part of it, as seen in the figure 42. The effect of the PWM was filtered from the

output by adding the small capacitor *C1* between the negative input and the output of the *U1*, making the circuit an integrator.

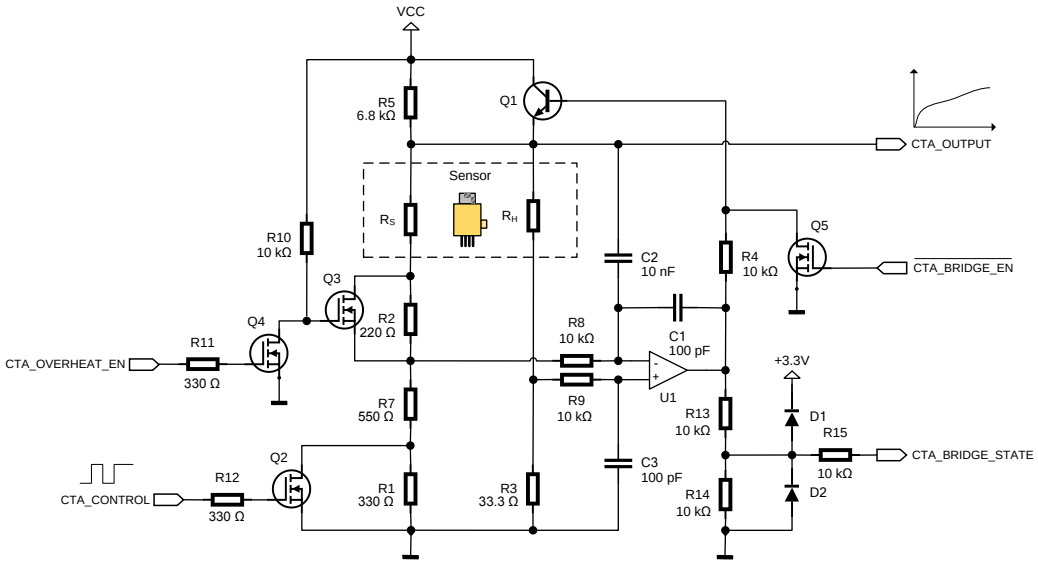

FIGURE 42. The second prototype of the CTA bridge

Due to the changes in the CTA bridge powering during calibration, the output of the *U1* was different than stated in the IST application note. The output was at zero level, or at the supply power (VCC) level depending on the inputs, and tripping near the balance state. To read the bridge state, the output of the *U1* connected to a digital input of the MCU through the voltage division *R13-R14* by using the CTA_BRIDGE_STATE signal. The logic values of the signal are listed in the table 19.

TABLE 19. CTA_BRIDGE_STATE output states

U1 input balance	**CTA_BRIDGE_STATE**
$IN- < IN+$	+3.3 V
$IN- \approx IN+$	Unstable / tripping
$IN- > IN+$	0 V

7.4 Mixture algorithm development

As stated in the theory of the CTA (King's law, equation 34 on the page 45), it produces a flow curve for a gas contributing all thermodynamic properties of that gas. The first assumption about mixtures was that the properties could be combined straight-forwardly by using only the mole fraction of the components. The algorithm development was started by measuring CTA output for several gases as characteristic curves. The first three gases were pure argon and helium, and a mixture containing 50 % argon and 50 % helium. By the mole fraction (equation 10 on page 21), the characteristic curve of the mixture can be calculated as a weighted average:

$$\dot{V}_{Ar+50He} = \frac{50\dot{V}_{Ar} + 50\dot{V}_{He}}{100} \quad [36]$$

where $\dot{V}_{Ar}$ is the characteristic curve of pure argon and $\dot{V}_{He}$ the characteristic curve of pure helium. Comparing the calculated curve to the measured one revealed that the measured values and the calculated values matched together almost exactly (figure 43). This made the first assumption plausible.

The measurements were continued with argon and carbon dioxide, and a mixture containing 82 % argon and 18 % carbon dioxide. They revealed that the mole fraction equation did not give a matching calculative curve for this mixture (figure 44).

By examining the heat transfer theory it was noticed that the relationship between gases in a mixture did not depend only on their mole fraction, but also on the relationship between their specific heat capacities. The specific heat capacity c_v is explained in the equation 24 on page 30 and it is directly proportional to the degrees of freedom. The conclusion was that when combining pure gas curves measured by the CTA, the relationships between the specific heat capacities should be taken into account.

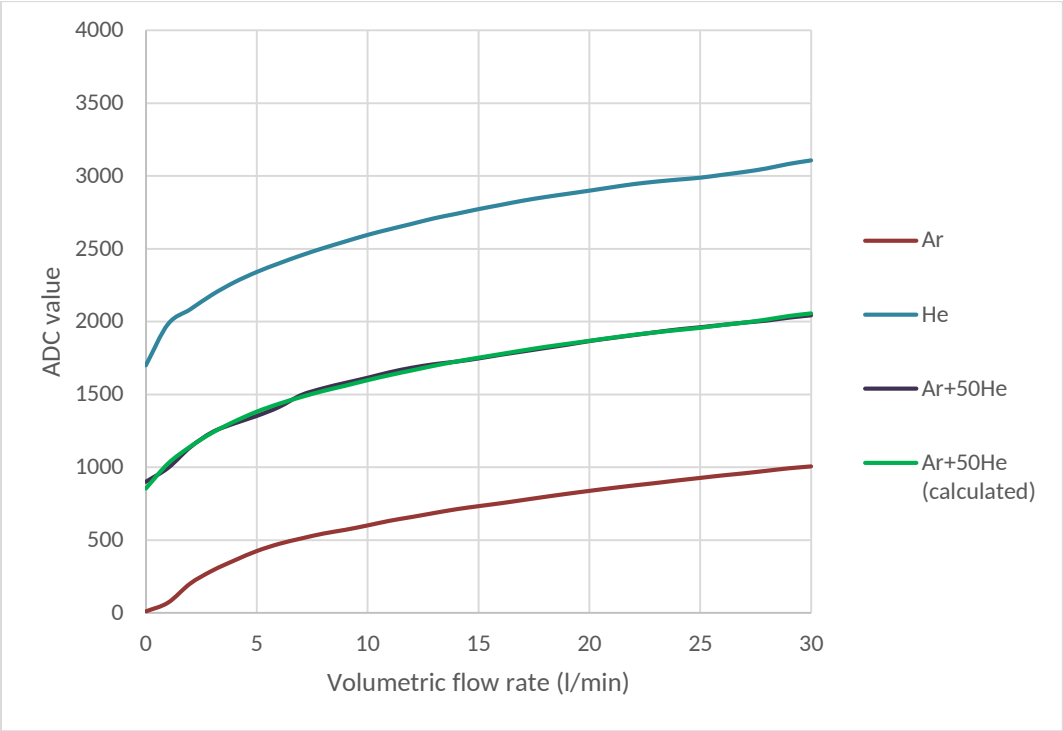

FIGURE 43. Argon-helium mixture, measured and calculated curve

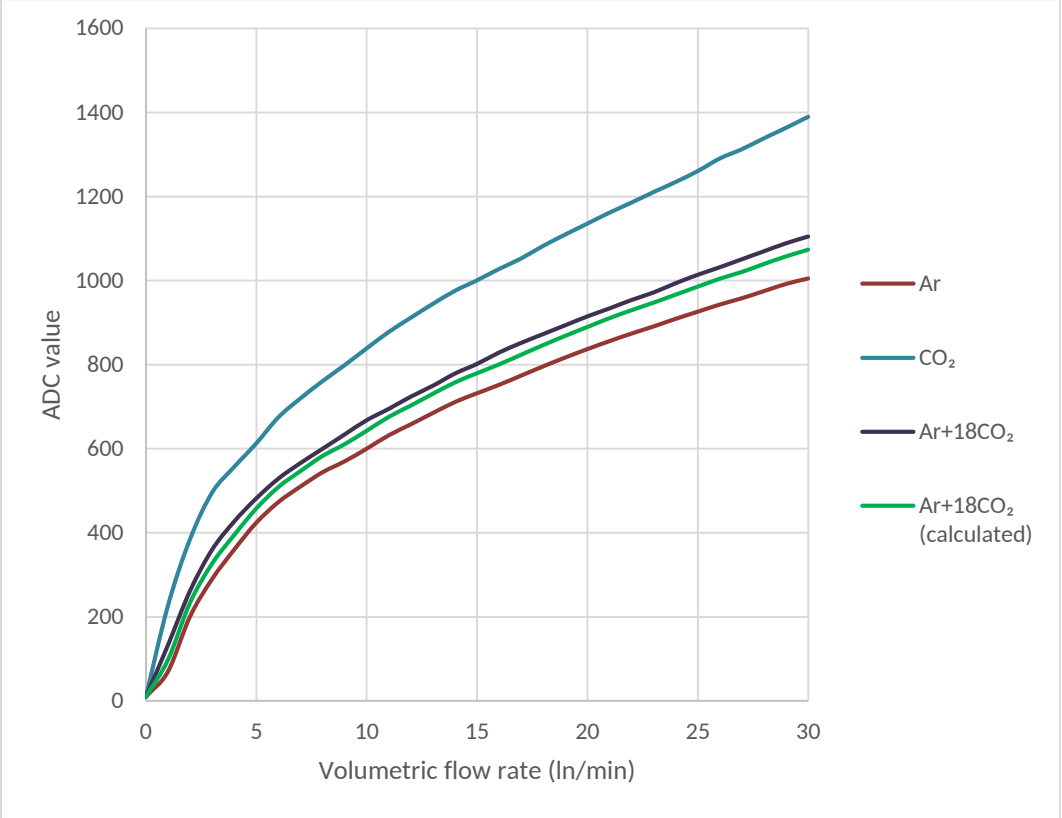

FIGURE 44. Argon and carbon dioxide, measured and calculated curve

Using the weighted average (by mole fraction) for the specific heat capacities of argon and helium gives:

$$c_{v,Ar+18CO_2} = \frac{82 \times c_{v,Ar} + 18 \times c_{v,CO_2}}{82 + 18}$$

Replacing the c_v by the corresponding equation:

$$\Longrightarrow \frac{f_{Ar+18CO_2} R_m}{2} = \frac{82 \times \frac{f_{Ar} R_m}{2} + 18 \times \frac{f_{CO_2} R_m}{2}}{100} \Bigg| \div \frac{R_m}{2}$$

and dividing both sides equally by the half of the universal gas constant results into:

$$\Longrightarrow f_{Ar+18CO_2} = \frac{82 f_{Ar} + 18 f_{CO_2}}{100}$$

where f_{Ar} is the degrees of freedom of argon, f_{CO_2} is the degrees of freedom of carbon dioxide, and $f_{Ar+18CO_2}$ is the degrees of freedom of the mixture. That can be expressed in general form as:

$$f_{mixture} = \frac{x_1 f_1 + x_2 f_2 + \cdots + x_n f_n}{x_1 + x_2 + \cdots + x_n} = \frac{\sum x_n f_n}{\sum x_n} \qquad [37]$$

where x_n is the fraction of the component in the mixture. Thus the heat capacities of the components in the mixture are solely relative to the degrees of freedom of those components.

In the first attempt, argon and helium had equal degrees of freedom and resulted into the matching curve by involving only the mole fraction of the components. In the second attempt the degrees of freedom of argon and carbon dioxide differed from each other significantly and the calculative curve did not match with the measured curve.

A new curve was calculated for the Ar+18CO_2 mixture by the means of the equation 37 and the degrees of freedom of argon and carbon dioxide:

$$\dot{V}_{Ar+18CO_2} = \frac{82 \times 3 \times \dot{V}_{Ar} + 18 \times 6.5 \times \dot{V}_{CO_2}}{82 \times 3 + 18 \times 6.5} \quad [38]$$

The resulted curve matched with the measured curve (figure 45).

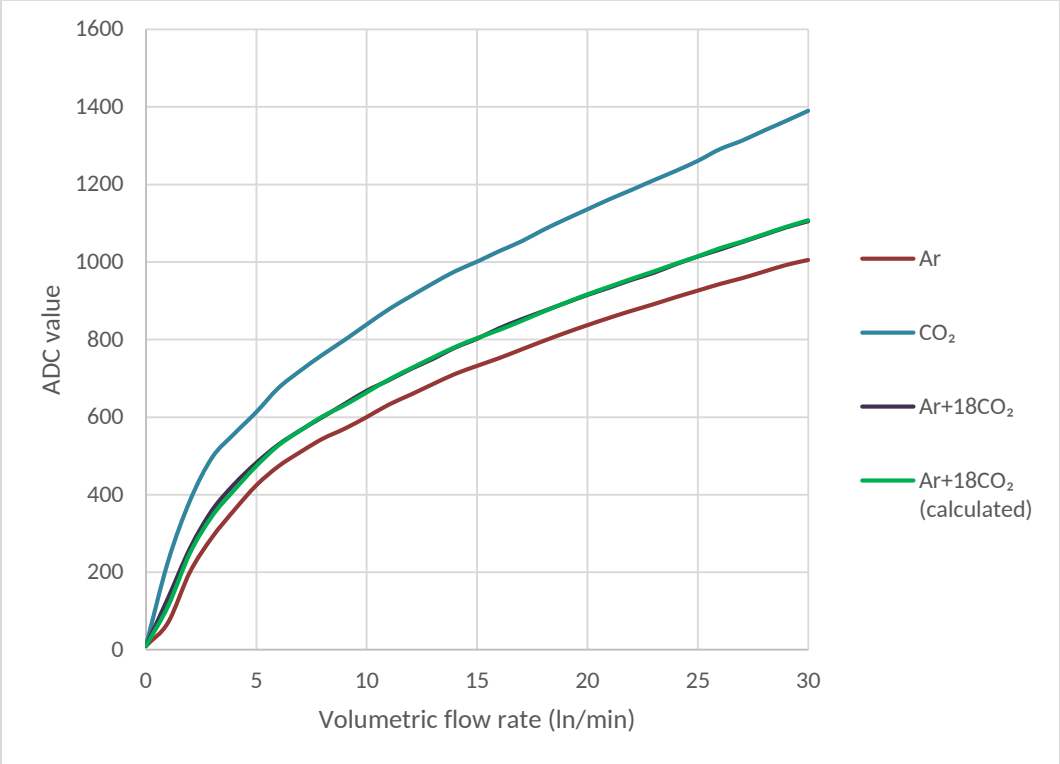

FIGURE 45. Argon and carbon dioxide, measured and calculated curve with contribution of degrees of freedom

The equation 38 of the curve can be written in a generic form for n gases as:

$$\dot{V}_{mixture} = \frac{\sum x_n f_n \dot{V}_n}{\sum x_n f_n} \quad [39]$$

where x_n is the fraction of the gas, f_n is the degrees of freedom of the gas and $\dot{V}$ is the characteristic curve of the gas. The equation was implemented to the sensor's software by using C language as shown in the figure 46.

```
static void
gfsCalcMixtureCurve(
        Sensor_GasFlow_Configuration_t *config,
        double *dof,
        const GFS_GasCurve_t *gasCurves,
        GFS_GasCurve_t *mixt
)
{
        int i,j;
        uint8_t x;
        double n,d,f;

        // Go through the gas curve.
        for(i=0;i<GFS_GASCURVE_SIZE;i++){
                n=d=0;
                // Go through all pure gas components.
                for(j=0;j<Sensor_GasFlow_PureGasCount;j++){
                        // Get the fraction of the component in the mixture.
                        x=config->Mixture[j];
                        // Check the component.
                        if(!x){
                                // This component doesn't contribute in the
                                // mixture
                                continue;
                        }
                        // Get the degrees of freedom of the component.
                        f=dof[j];
                        // Calculate the numerator.
                        n+=x*f*gasCurves[j].items[i].CTA;
                        // Calculate the denominator.
                        d+=x*f;
                }
                // Calculate the quotient and store it to the mixture curve.
                mixt->items[i].CTA=(uint16_t)FTOI(n/d);
        }
}
```

FIGURE 46. Example of program code for the mixture curve in C language

7.5 Software development

A microcontroller unit that was selected for this project was a 32-bit ARM® Cortex®-M3 core in a 100-pin BGA (ball-grid array) package. It was running at 72 MHz system clock and had 48 kB internal RAM (random access memory) and 256 kB internal program memory. The software was written in C language for RTXC Quadros RTOS (real-time operating system) and compiled with IAR Embedded Workbench® for ARM®. The system was built on Kemppi SystemBase architecture that provided direct interfacing with Kemppi's other system-class products by the means of a CAN (computer-area network) bus.

The system consisted of the CTA circuit, two NTC circuits for gas and housing temperatures, the microcontroller software, and the communication interface. The software was divided into logical parts implemented in separate units. The communication transactions and data types for the CAN bus were specified to be able to interface with other Kemppi products (figure 47).

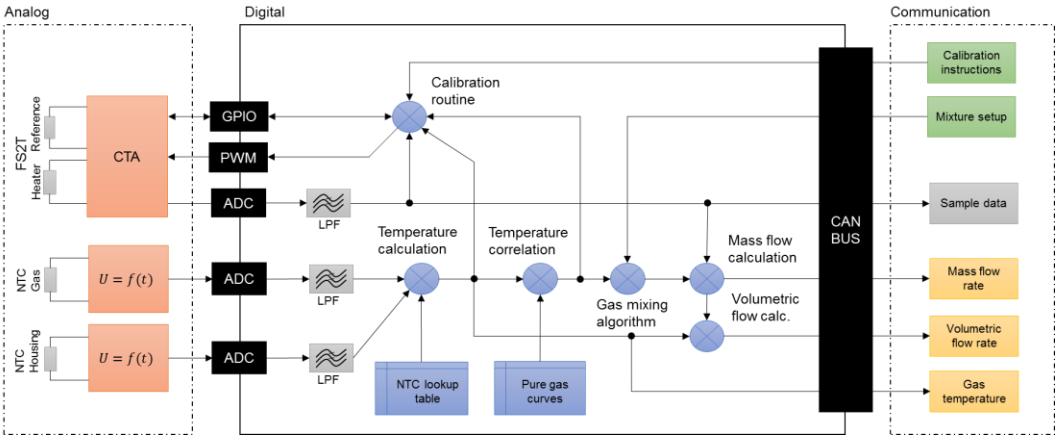

FIGURE 47. System architecture

A sensor framework was built to help support and management of different types of sensors, including the thermal mass flow sensor, different temperature sensors, and macroscopic software sensors (figure 48). The framework made an abstraction between the hardware and the sensor driver implementation so that the drivers did not need to be aware of the hardware. This made the system portable.

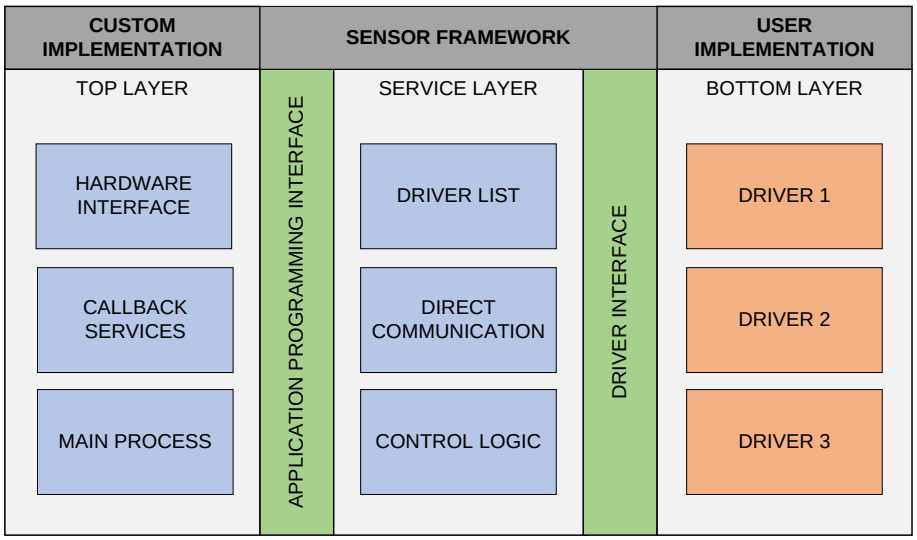

FIGURE 48. Structure of the sensor framework

A macroscopic driver for the gas flow sensor was implemented to the sensor framework including services for the thermal mass flow sensor, the CTA and the two NTC temperature sensors. The driver functionality included an initialization routine, a calibration routine and a regular (measurement) routine. The core process of the driver was implemented as a state machine that handled transmissions between routines and managed the states inside them (figure 49). The detailed logical structure of the regular routine is illustrated in the figure 50.

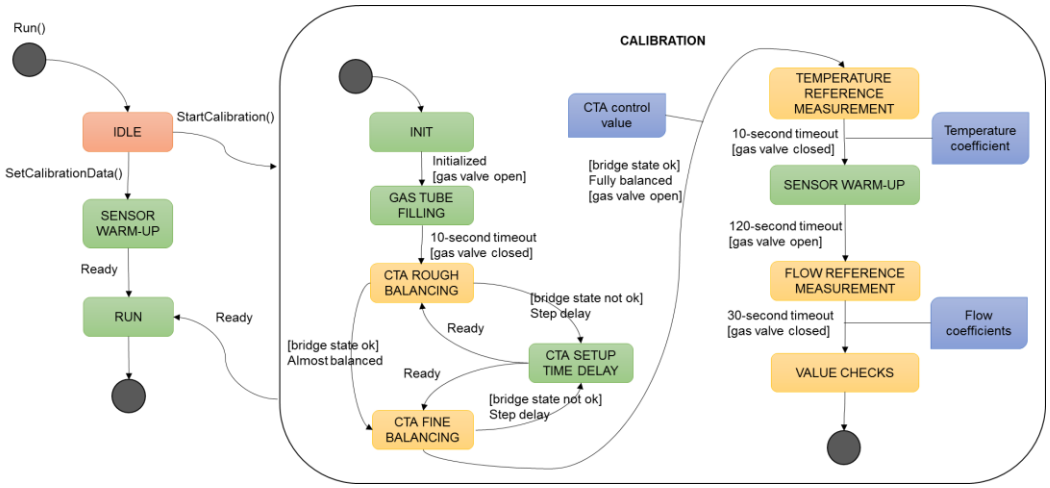

FIGURE 49. The state machine of the gas flow sensor driver

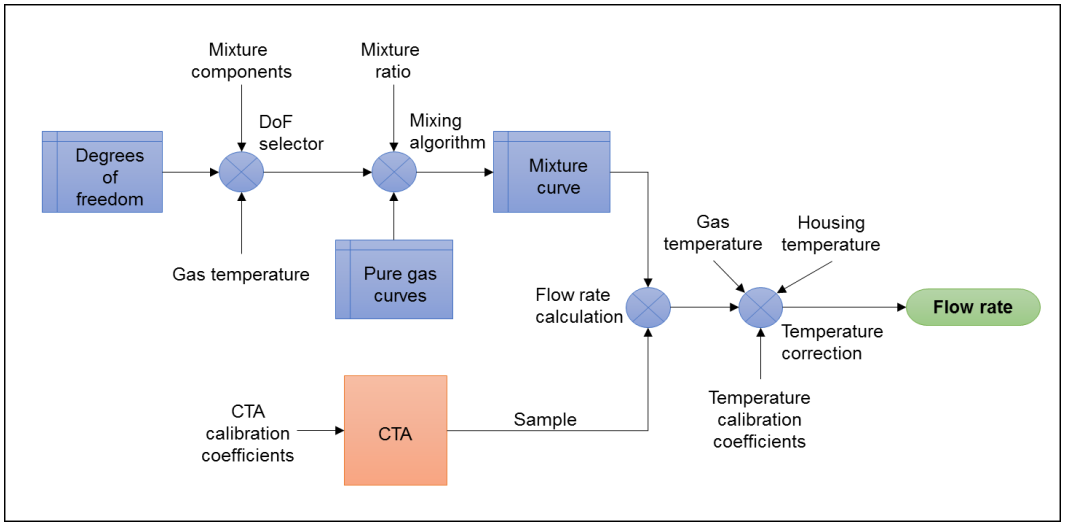

FIGURE 50. Detailed logical structure of the regular routine

7.6 Interfacing to the welding system

The new gas flow meter was equipped with the Kemppi system base software and the system bus interface. They enabled communication with Kemppi's system-class welding equipment. The gas flow meter required software changes in user interfaces and in the system base. An *A7 MIG Welder* system was prepared for testing the new device by adding the gas sensor configuration settings and flow rate monitoring to its web user interface. Settings included sensor on / off selection, flow detection level and mixture composition (figure 51). The gas flow rate was displayed in web user interface's welding display (figure 52).

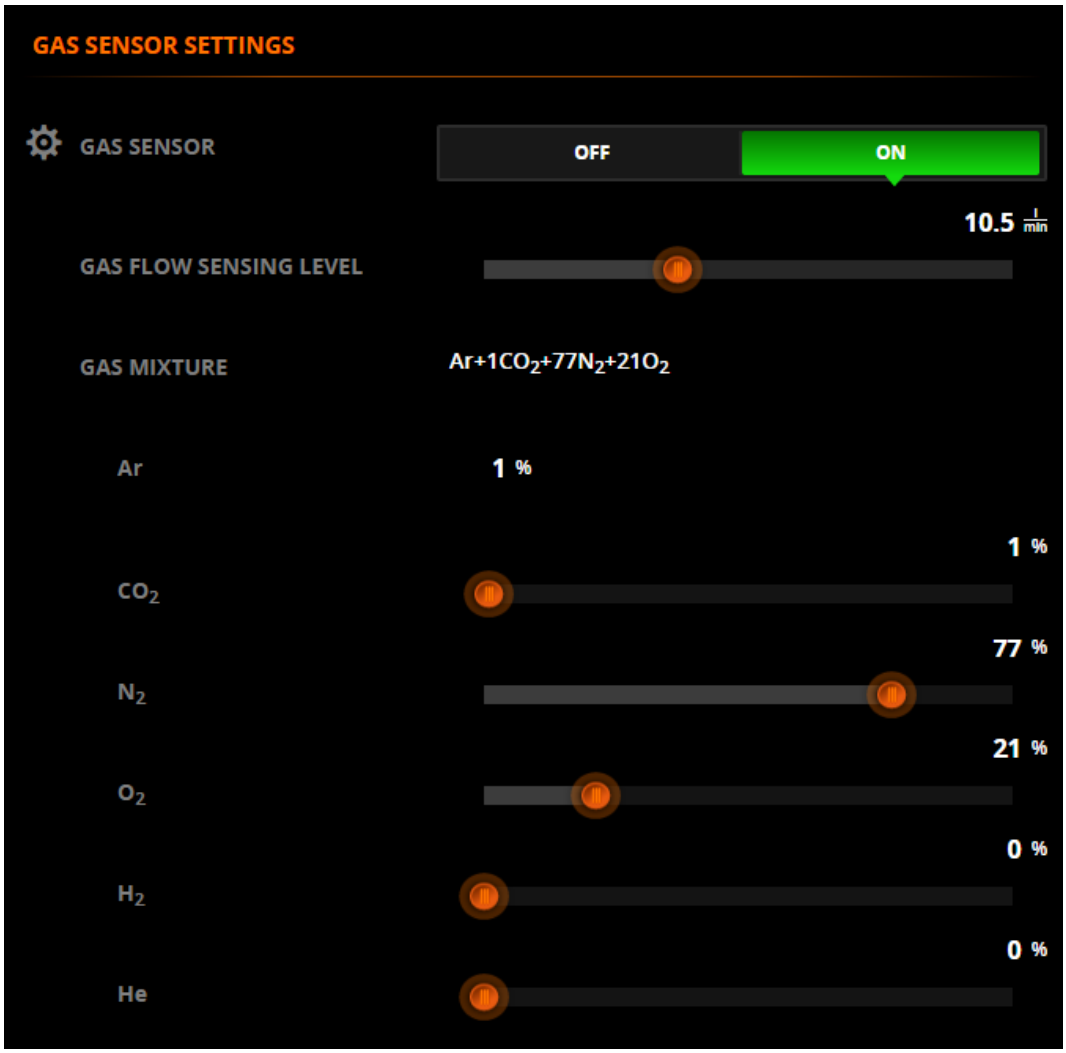

FIGURE 51. Gas sensor settings in A7 MIG Welder's web user interface

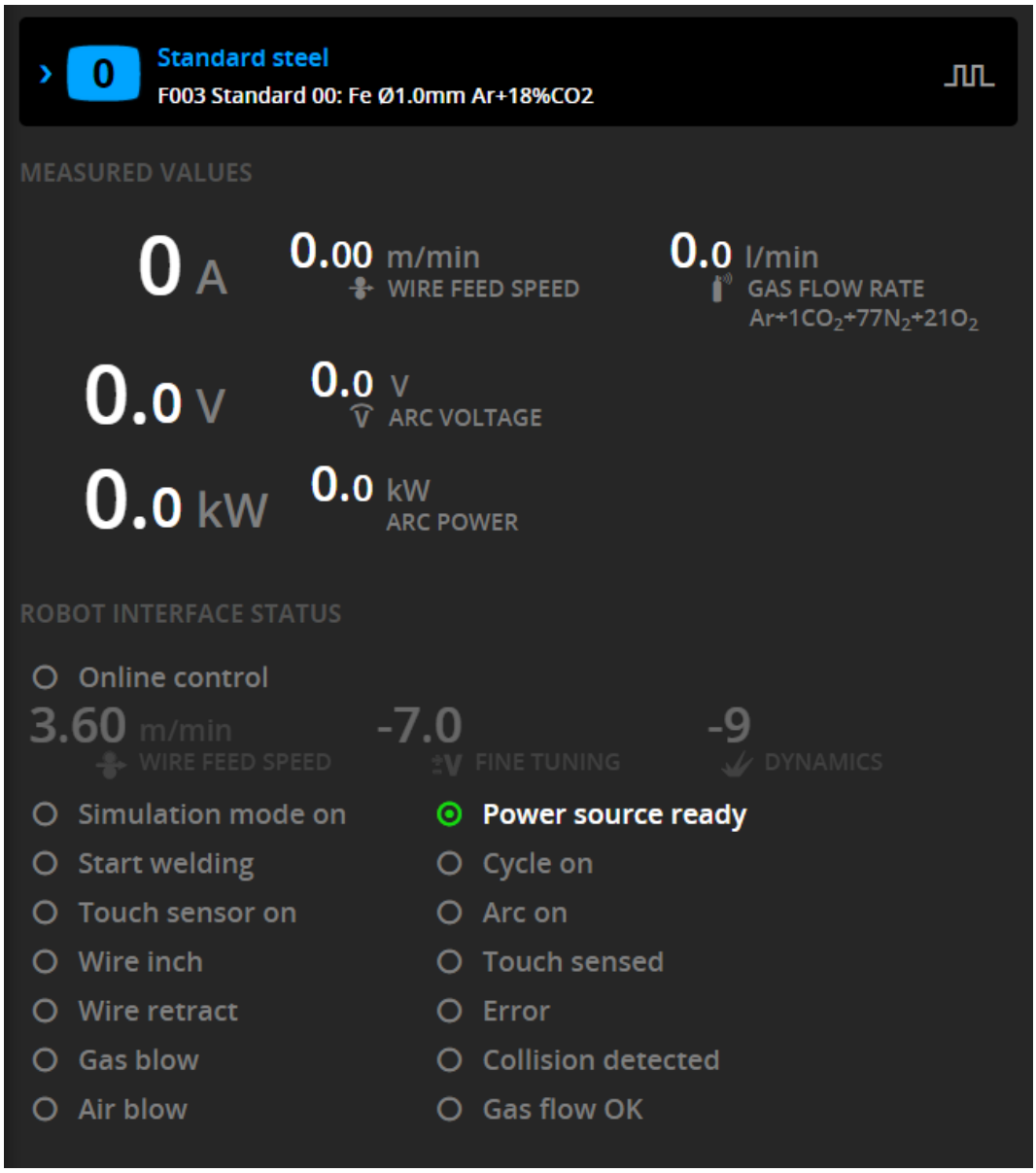

FIGURE 52. Welding display of the A7 MIG Welder's web user interface

The harness and gas hoses of the wire feeder of the A7 MIG Welder were changed so that the gas flow meter could be installed into it (figure 53). The gas flow meter was connected to the system bus by branching the harness. The old gas flow indicator was removed and the hoses connected to the new gas flow meter.

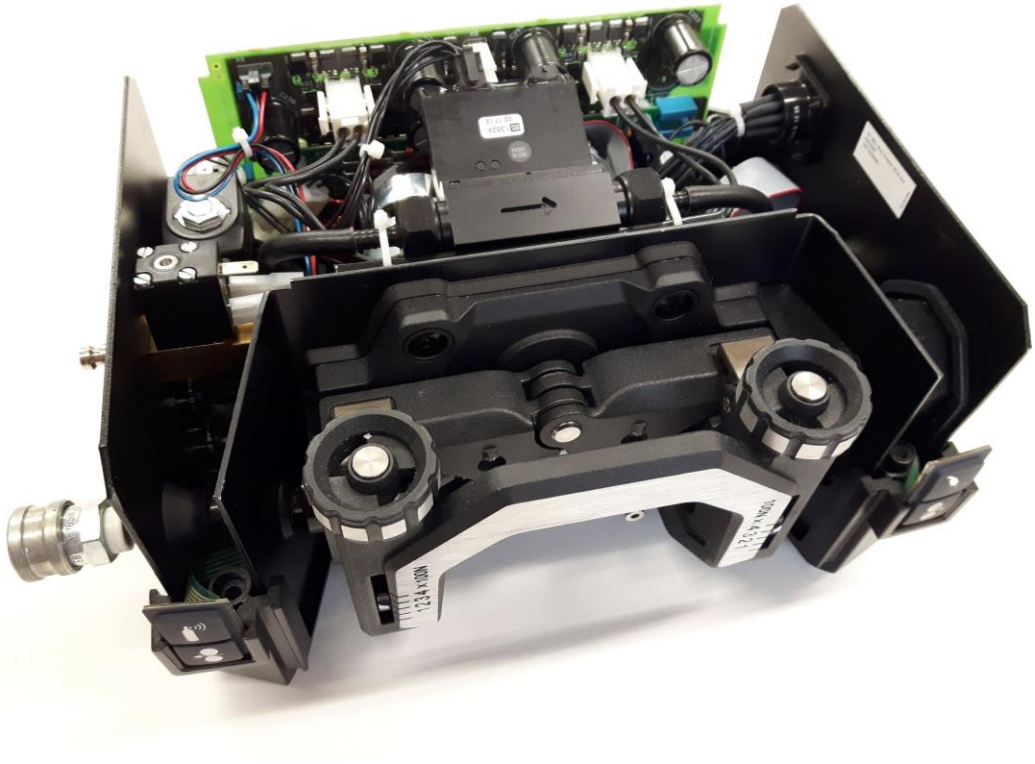

FIGURE 53. New gas flow meter installed in the wire feeder of the A7 MIG Welder

The wire feeder was connected to the *A7 MIG Power Source* by using an interconnection cable set. All other equipment and user interfaces were connected together internally inside the power source unit. The figure 54 illustrates the system bus distribution throughout the entire A7 MIG Welder system.

The A7 MIG Welder system is designed for automated welding and is controlled by a robot. The system was connected to a PC-based robot interface simulator for testing the gas flow meter. In the test the gas flow meter was configured for air (1% argon, 1% carbon dioxide, 77% nitrogen and 21% oxygen). Gas blow was switched on from the simulator to open a gas valve, and air blown through the gas flow meter. The web user interface displayed the gas flow rate according the blow strength (figure 55). The system was working properly with the new device.

FIGURE 54. System bus distribution in the A7 MIG Welder

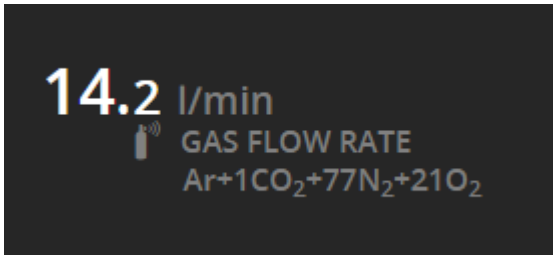

FIGURE 55. Air blow rate in the web user interface

8 CONCLUSIONS

The objective of this study was to research and develop a new gas flow meter for industrial welding. The main requirements for the product were connectivity, simple control, support for all welding gases including mixtures, and accuracy suitable for monitoring gas flow rate during welding.

As the result a new gas flow meter was developed. The device consisted of a printed circuit board and flow mechanics fixed onto the board. The construction was poured in resin (figure 56). The device utilized specific flow mechanics, a thermal mass flow sensor, a constant temperature anemometer (CTA), a microcontroller unit, and embedded software.

FIGURE 56. The final construction of the gas flow meter

The properties of gaseous mixtures were examined by using specific methods to combine the properties of pure components of the mixtures. This study listed different methods, such as Dalton model and Wilke mixture rule, with varying output accuracy. For the design of the flow mechanics, the worst case of the flow conditions was identified, and the mechanics designed and tested according to that case. The worst case came up with pure carbon dioxide in the highest pressure and lowest temperature of the interest. Therefor the mixture rules for kinematic properties were not required for to achieve the final construction.

By comparing different mass and volumetric flow measurement techniques, the thermal mass flow sensing was found the most suitable for this study. It was the simplest method to interface with digital electronics, and provided the most cost-effective solution. When connected to the CTA circuitry, the thermal mass flow sensor measured gas flow by measuring the convective heat transfer effect of the gas in motion.

The thermodynamic properties of the mixture were studied by examining the output of the CTA for pure welding gases and comparing the resulted characteristic curves together. The relationship between the characteristic curves revealed to be relative to both the mole fraction of the mixture and the degrees of freedom of the components of the mixture.

A new simple method was developed to calculate the flow rate for mixture gases. The method was based on pre-programmed characteristic curves of the pure gas components. In the software an algorithm read samples from the CTA by the means of an A/D converter, calculated the flow rate for the mixture gas based on an online configuration, and sent the result to the communication channel.

The new gas flow meter was successfully interfaced with Kemppi’s system class devices and could be operated as the fixed part of the welding system. The device could measure gas flow rate for any percentage-level mixture of the welding gases. Use of the gas flow meter required an external user interface to configure the sensor and to monitor the gas flow

rate, and the Kemppi system bus to connect the user interface to the device.

The device was very accurate in controlled conditions. However, the thermal mass flow sensor and the CTA appeared to be very sensitive to both common mode and differential temperature changes in between the gas temperature and the temperature of the flow mechanics (the housing of the thermal mass flow sensor) (figure 57). This affected to the flow measurement significantly and the device could not be approved to production without solving that issue.

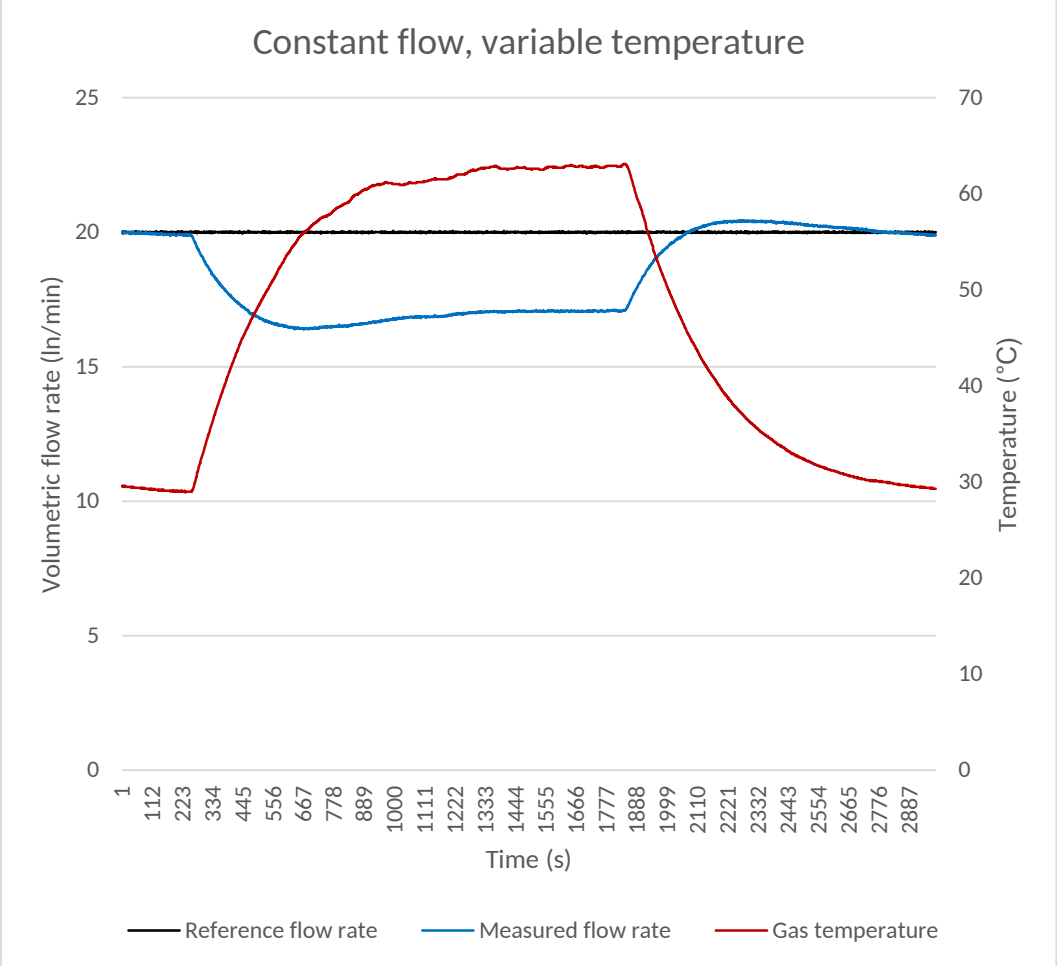

FIGURE 57. Flow rate error in gas temperature variation

The temperature effect to the flow rate could be compensated by using two temperature sensors, one measuring the gas temperature and another measuring the temperature of the housing. The device was equipped with those sensors, thus that issue could be solved by the means of calibration and compensation in the software. The investigation of this issue and the possible solution are beyond the scope of this study. Therefor the final accuracy of the product could not be examined within this study.

REFERENCES

Published references

AGA. 1998. Suojakaasukäsikirja. Espoo: Oy AGA Ab.

Alvesteffer, W., Baker, W., Cole, R. & Jacobs, D. 2007. A Brief History of the Thermal Mass Flow Meter and Controller. SVC Summer Bulletin 2010, 42-46.

Becken, O. 1969. Handbuch des Schutzgasschweißens. Part 1: Grundlagen und Anvendung. Düsseldorf: Deutscher Verlag für Schweisstechnik (DVS) GmbH.

Bohl, W. 1998. Technische Strömungslehre. 11th edition. Würzburg: Vogel Verlag und Druck GmbH & Co.

Borgnakke, C. & Sonntag, R. 2009. Fundamentals of Thermodynamics. 7th edition. Asia: John Wiley & Sons (Asia) Pte Ltd.

Çengel, Y. & Boles, M. 2015. Thermodynamics: An Engineering Approach. 8th edition. New York, NY: McGraw-Hill Education.

Çengel, Y. & Cimbala, J. 2010. Essential of Fluid Mechanics: Fundamentals and Applications. 2nd edition. New York, NY: McGraw-Hill.

Davidson, T. 1993. A Simple and Accurate Method for Calculating Viscosity of Gaseous Mixtures. Pittsburgh, PA: United States Department of the Interior, Bureau of Mines.

Demtröder, W. 2015. Experimental-physik 1: Mechanik und Wärme. 7th edition. Berlin: Springer Spektrum.

Holman, J. 2010. Heat transfer. 10th edition. New York, NY: McGraw-Hill.

Kuchling, H. 1999. Taschenbuch der Physik. München Wien: Fachbuchverlag Leipzig im Carl Hanser Verlag.

Lukkari, J. 1997. Hitsaustekniikka. Perusteet ja kaarihitsaus. 2nd edition. Helsinki: Opetushallitus.

Mangell, A. 2008. Flow measurement techniques. World Pumps Magazine 12/2008, 32-34.

Phillips, A. 1958. Welding Handbook. Section two. 4th edition. New York, NY: American Welding Society.

Young, H. & Freedman, R. 2012. University physics. 13th edition. San Francisco, CA: Addison-Wesley.

Electronic sources

Dantec Dynamics. 2017. Measurement principles of CTA. [referenced 24th January 2017]. Available: http://www.dantecdynamics.com/measurement-principles-of-cta

ElectronicsTutorials. 2017. Wheatstone Bridge. [referenced 24th January 2017]. Available: http://www.electronics-tutorials.ws/blog/wheatstone-bridge.html

IST AG. 2016a. AN Flow 001: Constant Temperature Anemometer (CTA). Application note. [referenced 14th November 2016]. Available: http://www.flowcontrolnetwork.com/ext/resources/files/assets/whitepapers/FC-0412-ISTPaper.pdf

IST AG. 2016b. FS2 Thermal Mass Flow Sensor. Data sheet. [referenced 17th November 2016]. Available: http://www.ist-usadivision.com/objects/media/data-sheets/product/flow/FS2.pdf

IST AG. 2016c. Thermal Flow Sensors. Application note. [referenced 17th November 2016]. Available: http://www.ist-usadivision.com/objects/media/data-sheets/application-notes/flow/Thermal%20Flow%20Sensors.pdf

Kemppi. 2016. A7 MIG Welder Operating Manual. [referenced 17th January 2017]. Available: http://d3dbtvmfwwhlf2.cloudfront.net/pub/Offering/Operating+manuals/Equipment/Automated+welding/Robotic/A7+MIG+Welder/a7-mig-welder-operating-manual-en.pdf

NIST-JANAF. 2017. NIST-JANAF Thermochemical Tables. [referenced 9th March 2017]. Available: http://kinetics.nist.gov/janaf/

NXP. 2017. LPC2364/65/66/67/68 Product data sheet. [referenced 18th January 2017]. Available: https://www.nxp.com/documents/data_sheet/LPC2364_65_66_67_68.pdf

WeldEye. 2016. Universal welding management software. [referenced 22th November 2016]. Available: http://www.weldeye.com/en-US/software/welding-management-software/weldeye/

Standards and patents

IEC-60974-5. 2013. Arc welding equipment – Part 5. Wire feeders. Geneva, Switzerland: IEC Central Office.

SFS-EN ISO 14175. 2008. Welding consumables – Gases and gas mixtures for fusion welding and allied processes. Helsinki, Finland: Finnish Standards Association.